Ultrafast Strong Field Driven 2D and 3D Semiconductors – Higher Order Many-body Correlations

Jerome V Moloney
Arizona Center for Mathematical Sciences
Wyant College of Optical Sciences
University of Arizona, Tucson AZ 85721

Research Team: Miroslav Kolesik, Jorg Hader, Colm Dineen, Andrew Parks (Postdoc), Simon Tsaoussis (Student)

Support: AFOSR FA9550-25-1-0065 (Current), FA9550-19-1-0032, FA9550-21-1-0463

Multi-harmonic spanning nonlinear X-wave: extreme long wave infrared dispersive shock regularization – Xenon Gas

- M. Hastings, P. Panagiotopoulos, M. Kolesik and JVM Phys. Rev. Lett. Vol. 132, 253801 (2024)
- Michael Hastings PhD (2024)

- Spectrally resolved far-field
- Transition from modified Kadomtsev-Petviashili to NLS type behavior

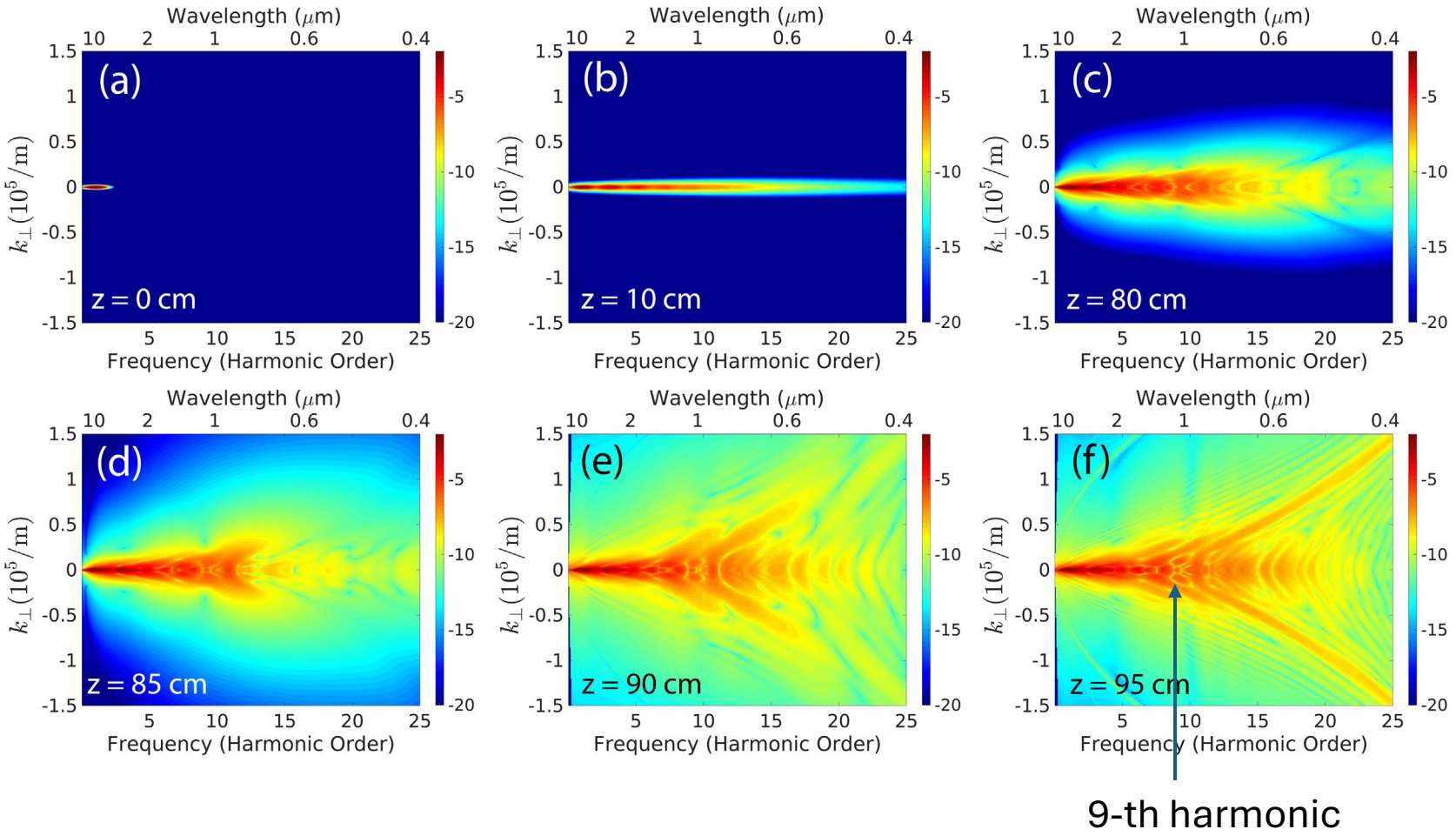

Multi-harmonic spanning nonlinear X-wave:extreme long wave infrared dispersive shock regularization

On-axis field carrier wave

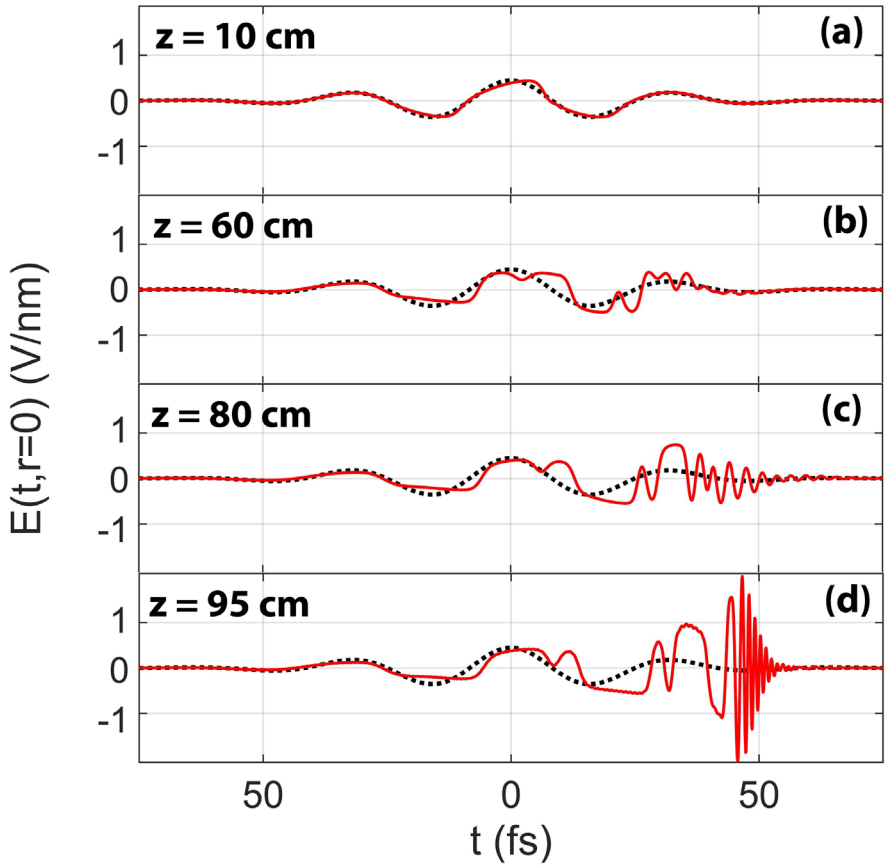

Asymptotic X-wave and Filter

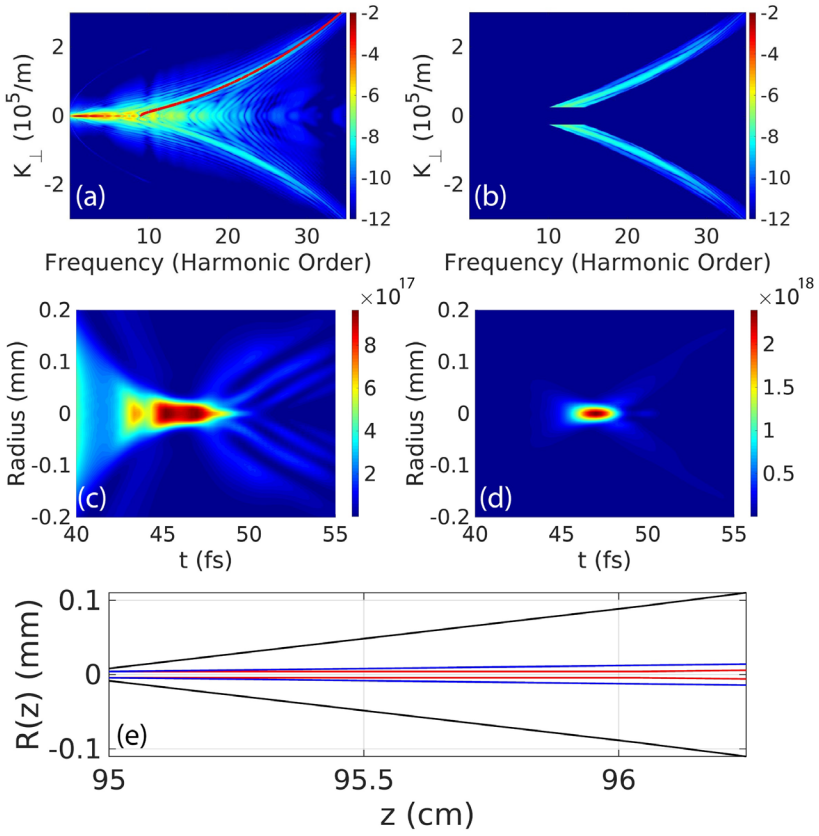

9-th harmonic seeded X-wave propagates linearly and nonlinearly over more than 100 Rayleigh lengths.

Coupled Cavity Multi-GHZ mode-locked SDLs

Simon Tsaoussis , S. Addame (Sandia), Jason Jones and JVM Optics Letters Vol. 49, 1688-1691,(2024)

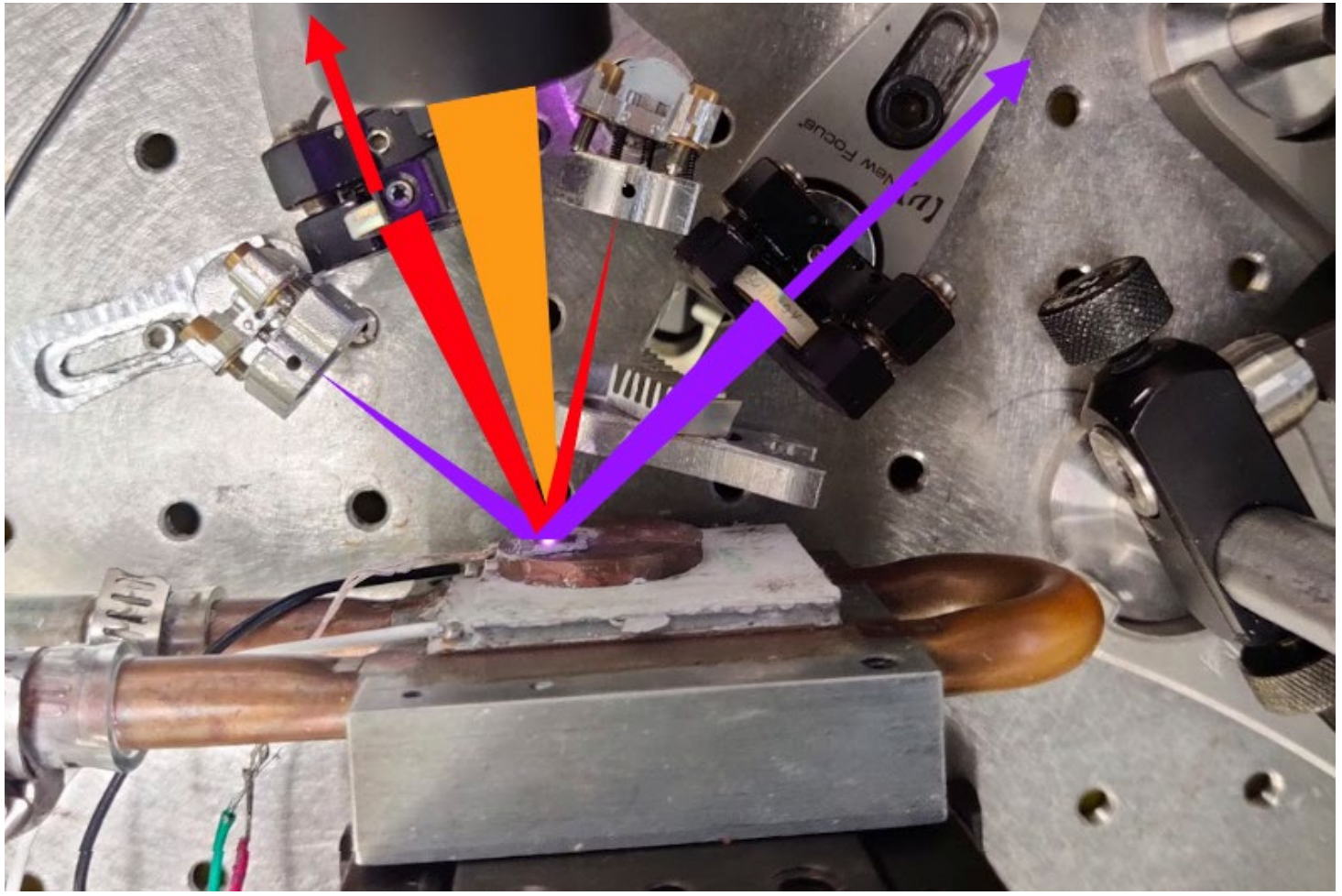

Pump

Inner Cavity

Outer Cavity

Results

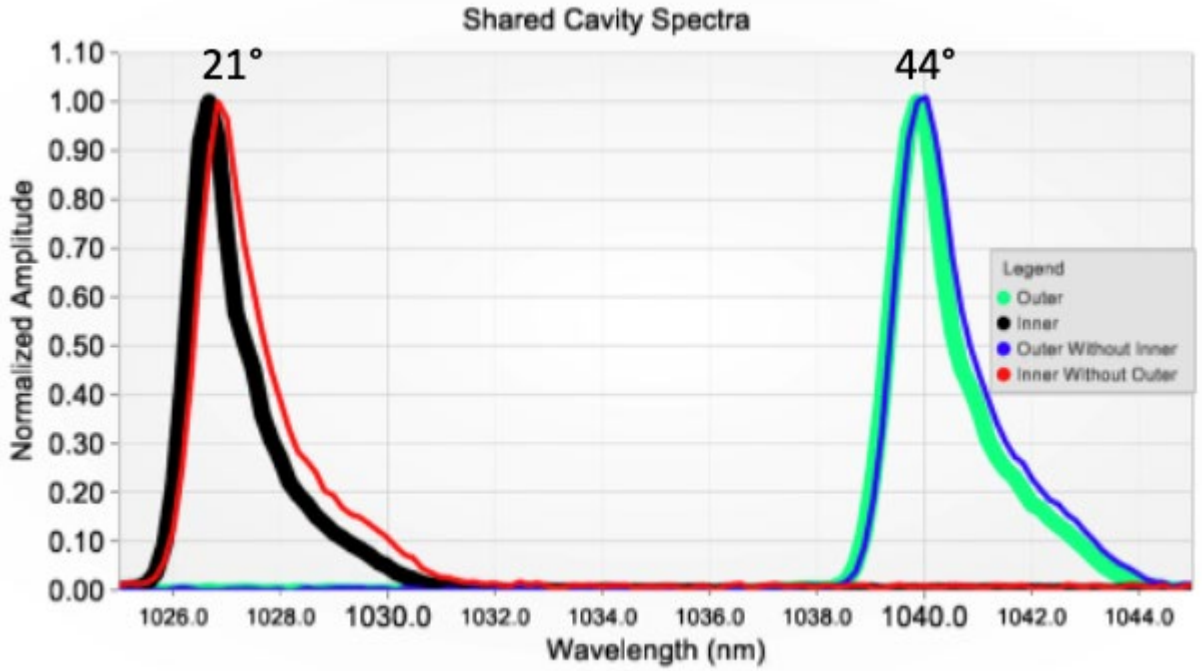

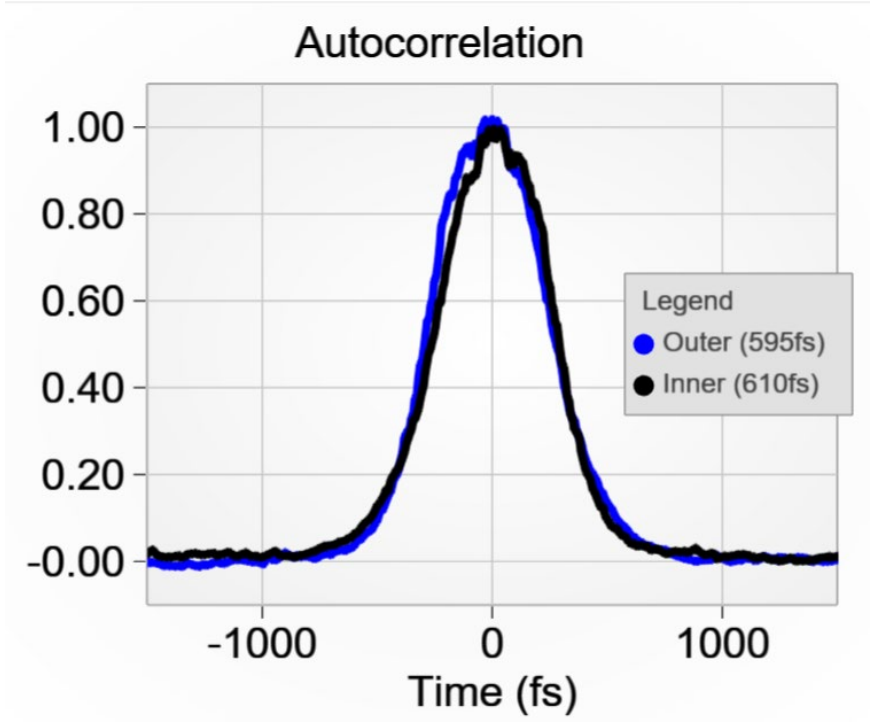

And they are both simultaneously modelocked

	Rep Rate	Pulse Width	λ_0	Avg Power
Inner	2.110 GHz	595 fs	1027nm	28mW
Outer	2.170 GHz	610 fs	1040nm	32mW

Classical Optics: Angle Enforced Spectral Filter

Early Microscopic Simulations restricted to a single effective QW

- I. Kilen, J. Hader, **J. V. Moloney**, and S. W. Koch "Ultrafast nonequilibrium carrier dynamics in semiconductor laser mode locking" *Optica*, **192**-197 (2014)

Partial coherence of RPG Periodic Stack enforces Angle selective wavelength filtering

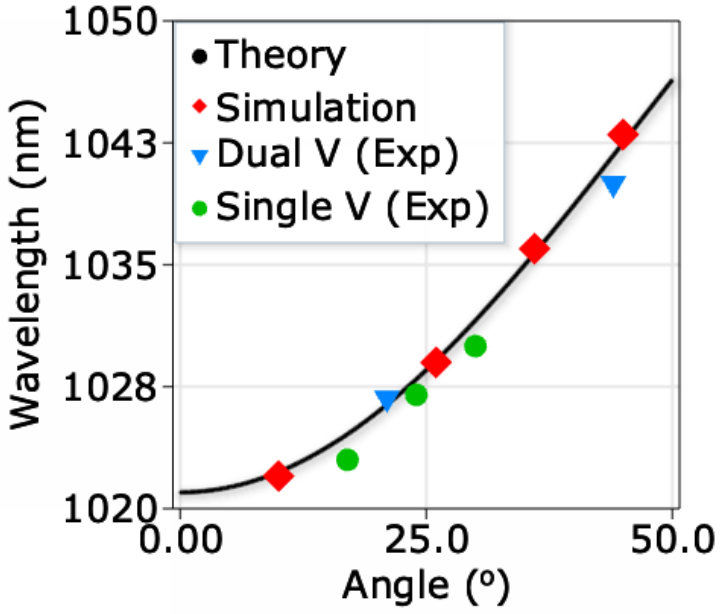

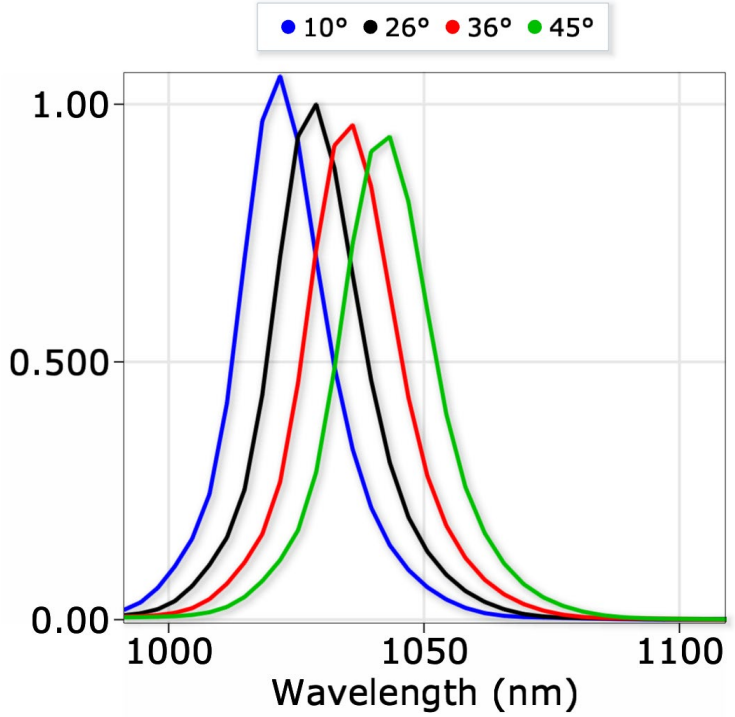

Utility patent 18/750,159 filed June 2024.

Dual V-Cavity Asymptotic State- Stable Mode-locking

- Finite grating basis expansion of SBE microscopic polarization and populations.

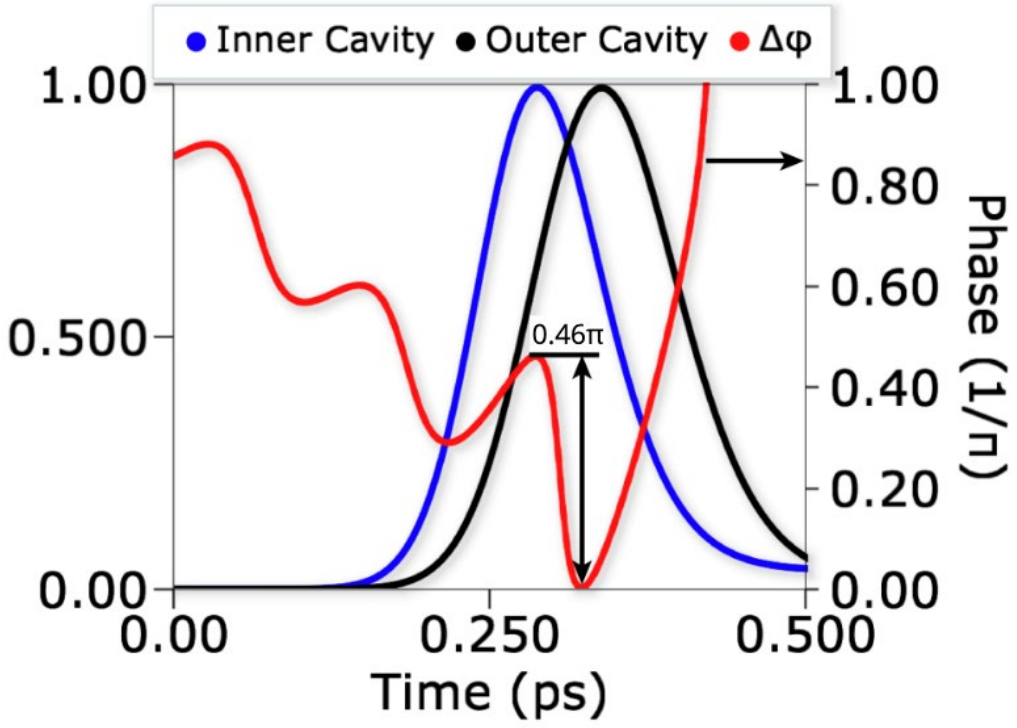

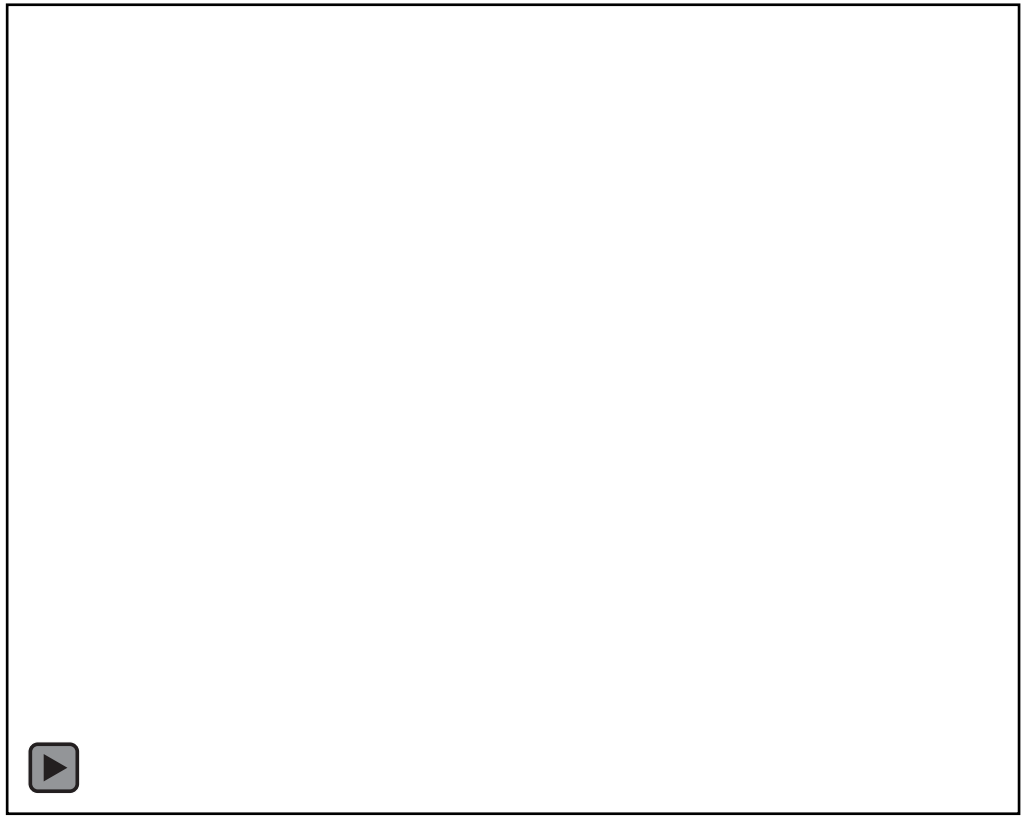

Triple V-cavity In-plane View

Three Cavity Experiment **Idea**

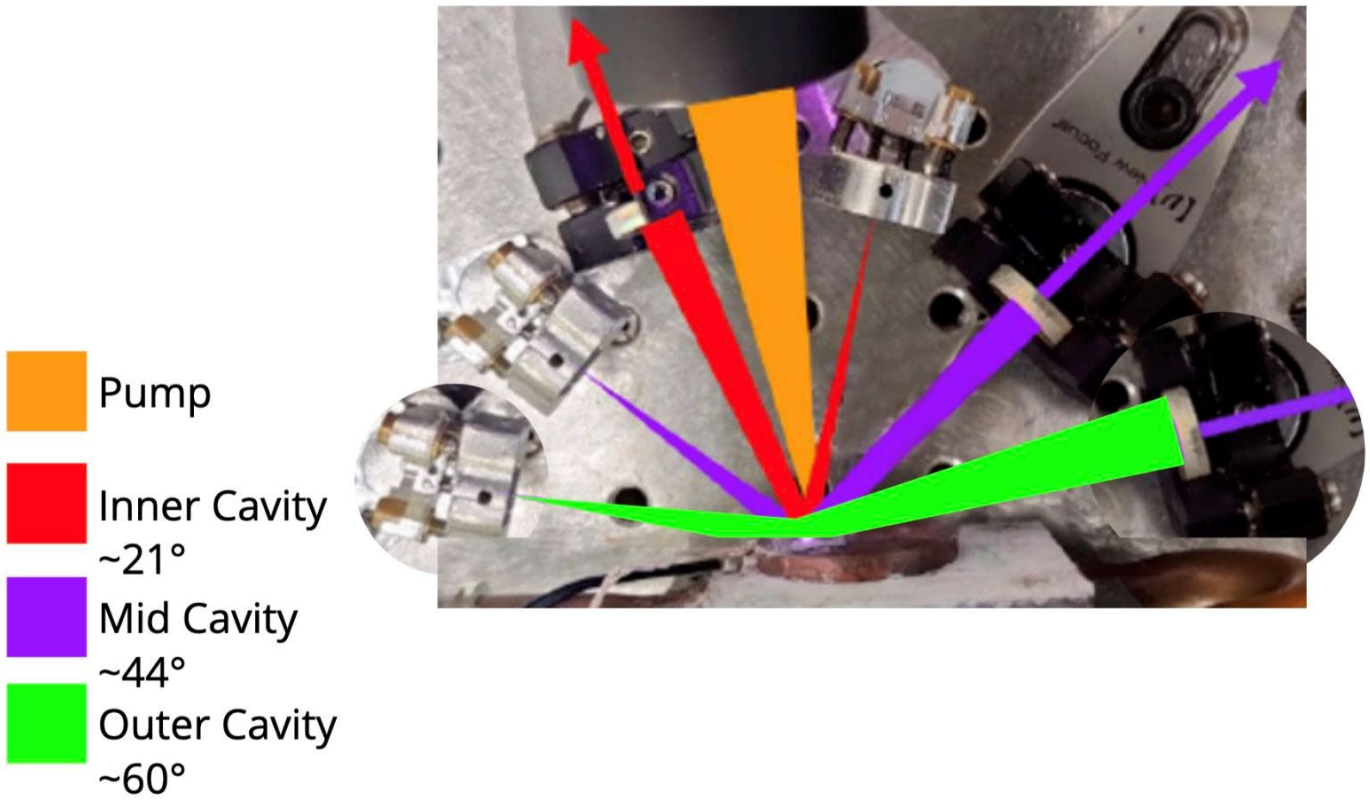

In-plane Triple V-cavity – Quasi-stable Mode-locking

- Need to increase pump and balance outcoupling losses in each arm for stable mode-locking
- Snapshot at t=1.17 ns

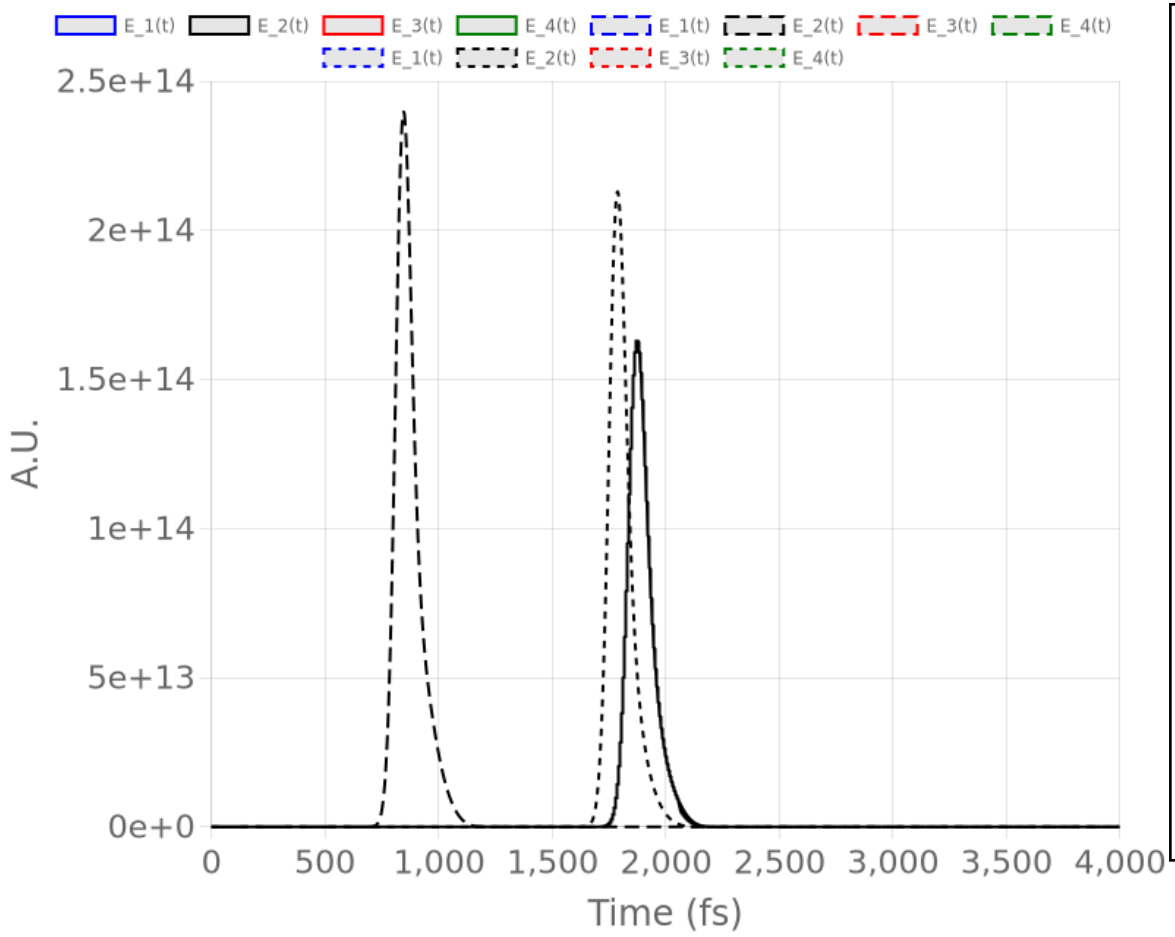

Unstable Asymptotic State – Spectral Overlap

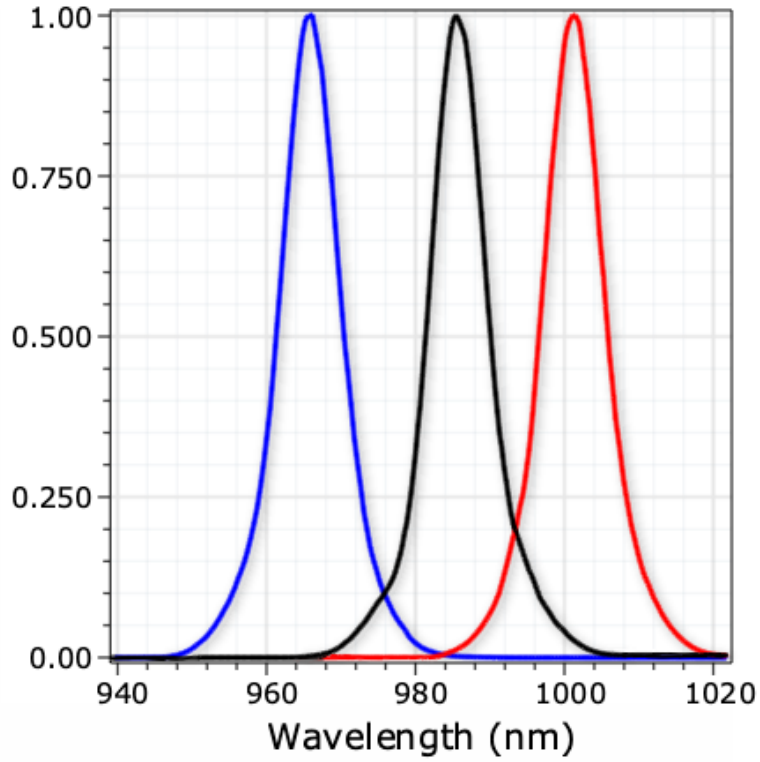

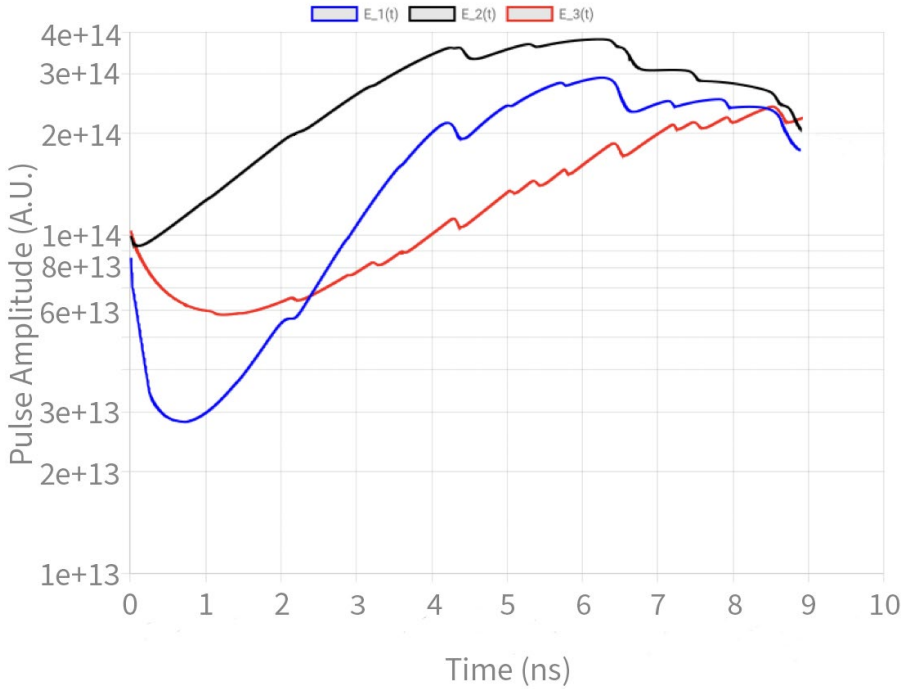

High Field Robust, Gauge Invariant SBE solvers

- structure gauge independent SBE solver (**sgi-SBEs)**

- Explicit time-stepping algorithm for evolution of density matrix

$$\rho_{nm}(\mathbf{k}_t, t) = \sum_{m'n'} \langle n\mathbf{k}_t | n'\mathbf{k}_0 \rangle \rho_{n'm'}(\mathbf{k}_0, t_0) \langle m'\mathbf{k}_0 | m\mathbf{k}_t \rangle e^{-i\varepsilon_{nm}(\mathbf{k}_t)\,(t-t_0)}$$

M. Kolesik et al. PRA 106, 06351, (2022)

- - Phases of instantaneous Bloch eigenstates are irrelevant and do not affect calculations

- Gauge invariant SBEs (**GI-SBEs**)
  - SBEs transformed to eliminate gauge-dependent quantities
  - 2-band GI-SBE for interband coherence:

AM Parks et al, PRL **131**, 236902 (2023)
AM Parks et al, JOSA B **42**, B47 (2024)

$$\partial_t \rho_{cv} = \mathbf{E}(t) \cdot \nabla_k \rho_{cv} - i[\varepsilon_{cv} + \mathbf{E}(t) \cdot \mathbf{R}_{cv}]\rho_{cv} + iE(t)|d_{cv}|(\rho_{cc} - \rho_{vv})$$

- - Berry connections and TDM phase replaced by a gauge-invariant quantity known as the shift vector $\mathbf{R}_{cv}(\mathbf{k})$

- Both approaches are particularly well-suited to topological materials, in which the existence of a smooth+periodic Bloch phase is fundamentally prohibited by so-called topological obstruction

QWZ model for Chern insulator

- HHG in topological materials, challenge of constructing a smooth Bloch gauge
- Robust SBE solvers* are insensitive to Bloch phases, and can simulate HHG with very high accuracy
- Example: simple model of Qi-Wu-Zhang (QWZ) for 2-band Chern insulator on 2D square lattice
  - Satisfies inversion symmetry, but breaks time-reversal (TR) symmetry
  - Model parameters control transition between trivial and topological phase

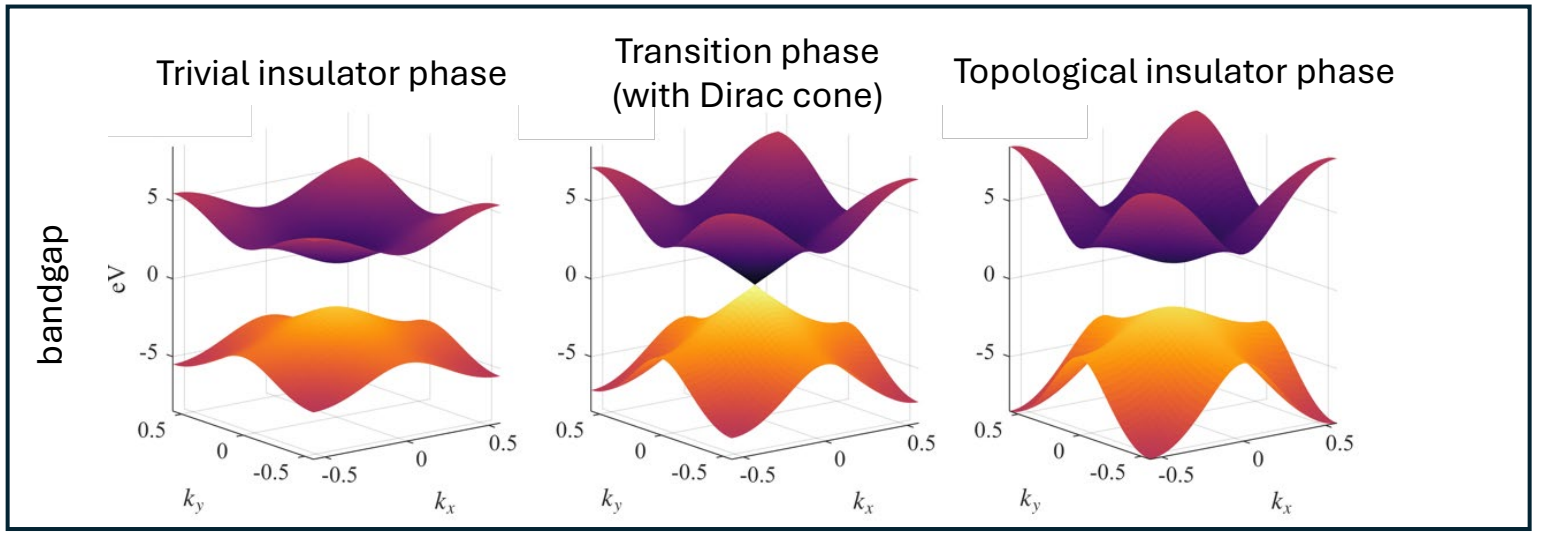

*References
AM Parks et al, PRL **131**, 236902 (2023)
AM Parks et al, JOSA B **42**, B47 (2024)

Miro's sgiSBEs refs

HHG in QWZ model

- Successful high-fidelity HHG simulations in QWZ model in both trivial and topological phases
  - Two different orientations of a linearly polarized driving laser
  - Total yield and output ellipticity of generated harmonics are calculated with high precision

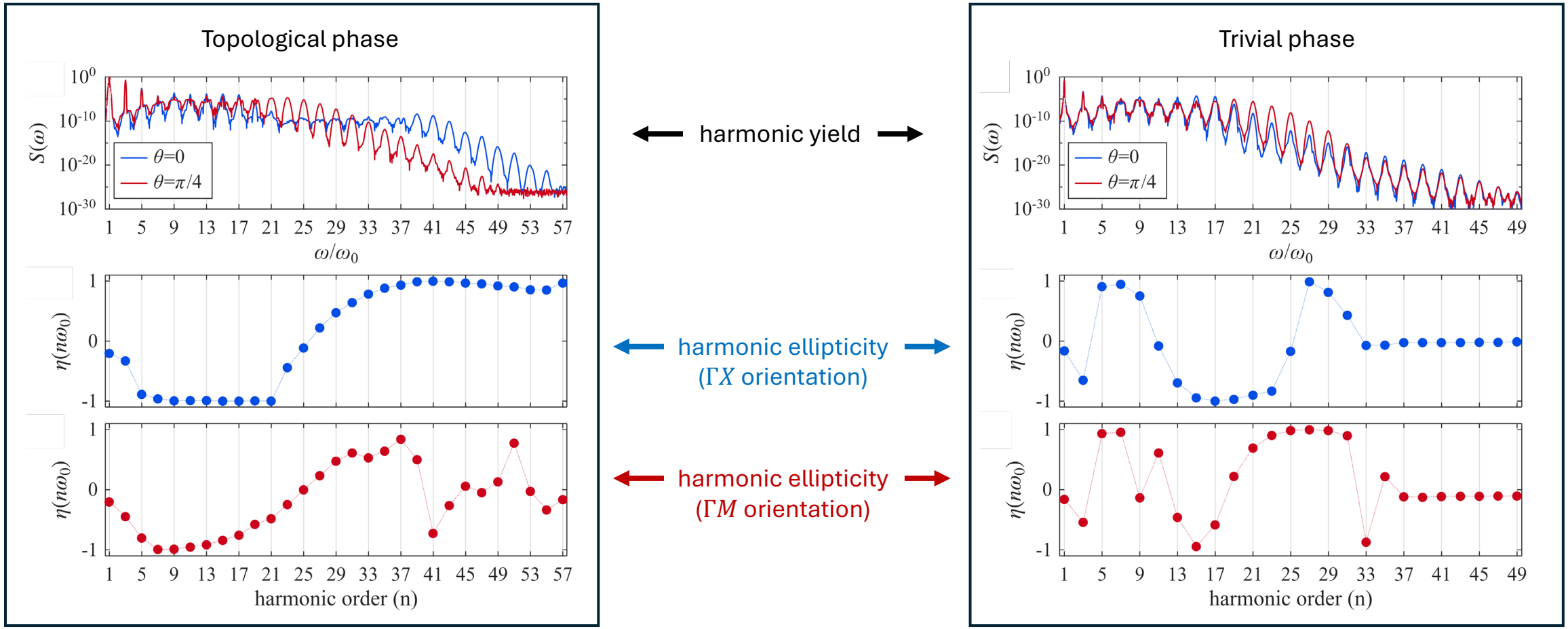

HHG in QWZ model

- Efficient and robust numerics allow us to investigate k-space origin of HHG phenemona
- Excite with linearly polarized driver along $\hat{x}$; restrict simulation to a region of extent L_y along $\hat{y}$-direction
  - 1D approximation fails to capture multiple-plateau structure of HHG spectrum

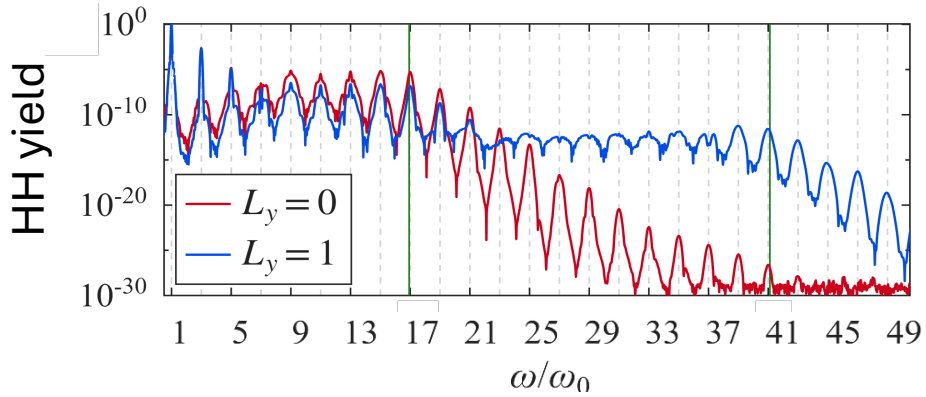

L_y=0 → 1D approximation
L_y=1 → full 2D Brillouin zone

- Increasing simulation region shows that 2nd plateau originates from interference throughout entire BZ

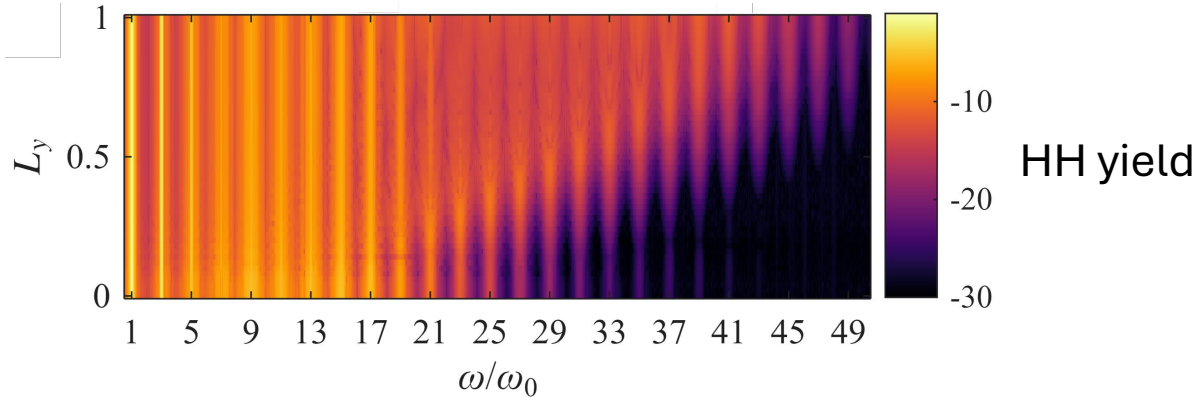

Extreme Nonlinear Optics in TMDCs

Transition Metal Dichalcogenides MX_2

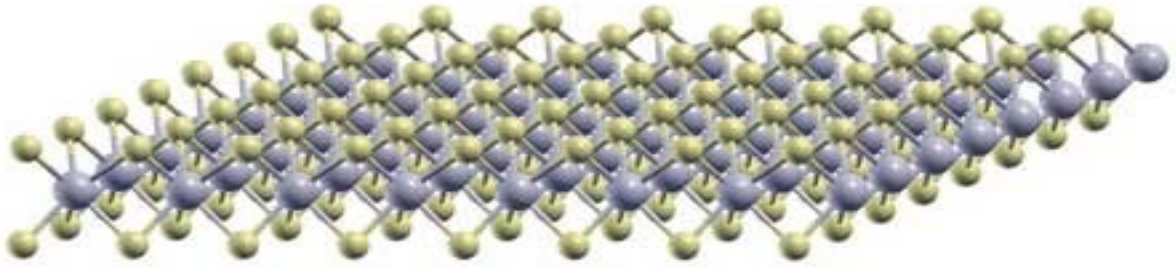

DFT Input Bandstructure

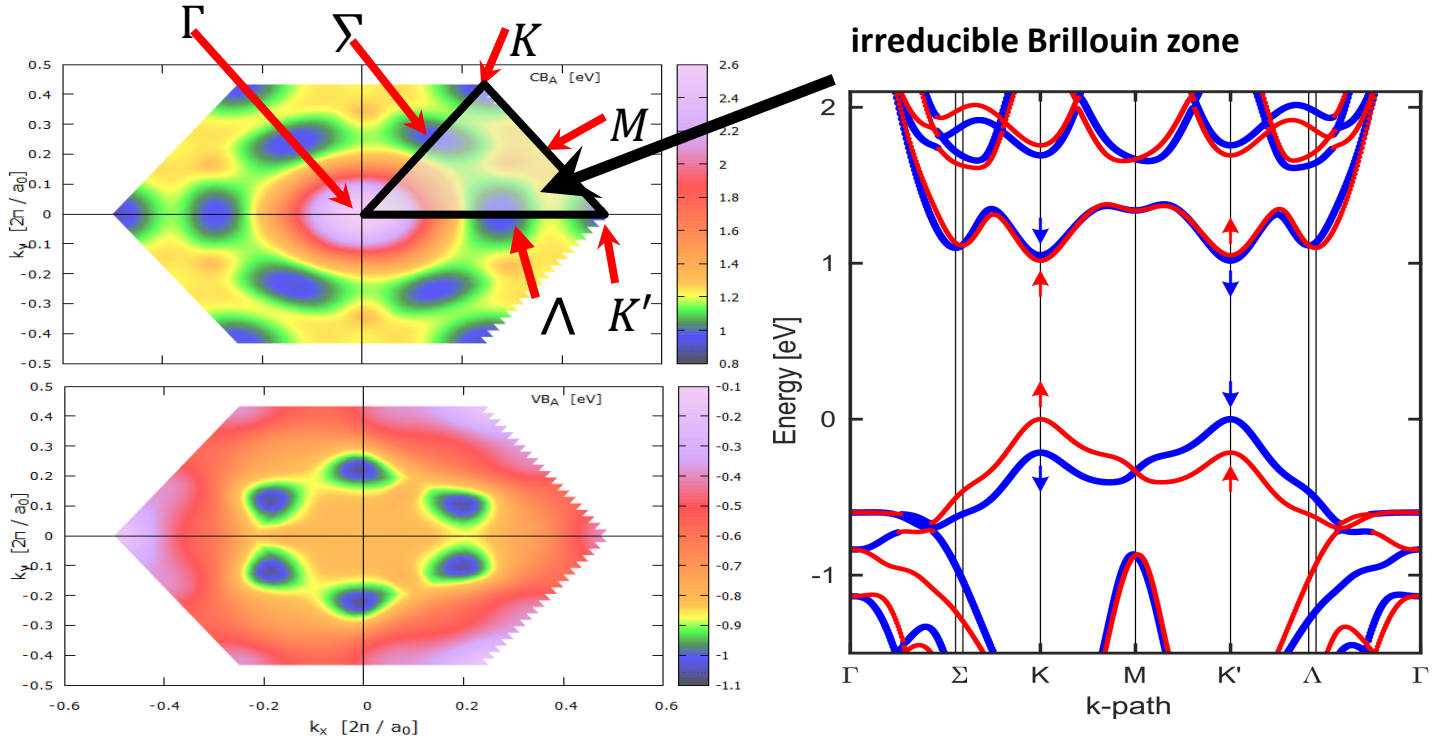

Semiconductor Luminescence Equations

J. Hader and J.V. Moloney, "Photo Luminescence and Radiative Carrier Losses in Monolayer Transition Metal Dichalcogenides," Nano Lett. 24, 5231-5237 (2024)

Equation of motion for photon assisted polarizations:

$$i\hbar \frac{\partial}{\partial t} \Pi^{ij}_{\mathbf{k},\sigma} = \sum_{i',j'} \left[\mathcal{E}^{ii'}_{\mathbf{k}} \delta_{jj'} - \mathcal{E}^{jj'}_{\mathbf{k}} \delta_{ii'} \right] \Pi^{i'j'}_{\mathbf{k},\sigma}$$

$$- \left(1 - f^{i}_{\mathbf{k}} - f^{j}_{\mathbf{k}}\right) \sum_{i',j',\mathbf{k}'} V^{ij'ji'}_{\mathbf{k}-\mathbf{k}'} \Pi^{i'j'}_{\mathbf{k}',\sigma}$$

$$- \sum_{\mathbf{k}'} \left[\Gamma^{j}_{\mathbf{k},\mathbf{k}'} + \Gamma^{i}_{\mathbf{k},\mathbf{k}'} \right] \Pi^{ij}_{\mathbf{k}+\mathbf{k}',\sigma}$$

$$- A_{\sigma}(t) \mu^{ij}_{\mathbf{k},\sigma} \left[f^{i}_{\mathbf{k}} f^{j}_{\mathbf{k}} + \sum_{i',j',\mathbf{k}'} C^{i'jij'}_{\mathbf{k},\mathbf{k}'} \right]$$

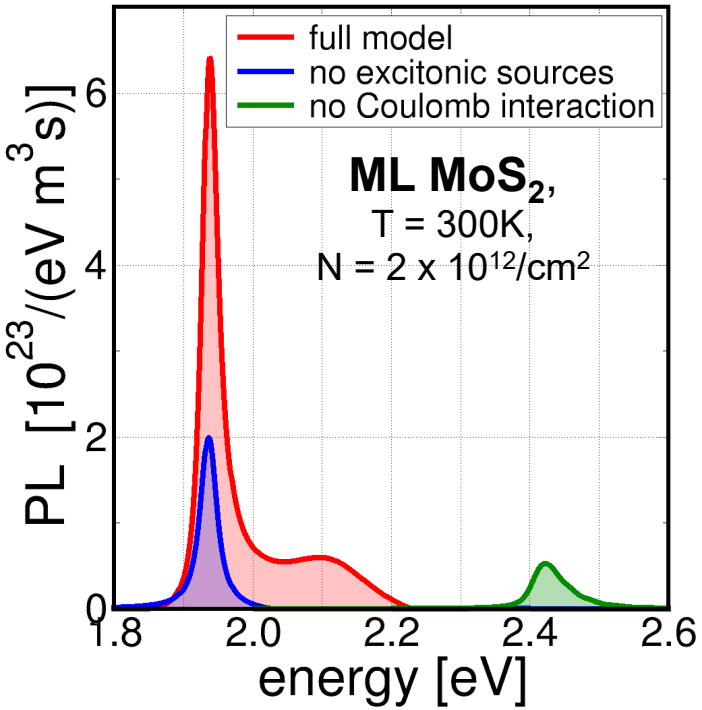

excitonic resonances, bandgap renormalization

scatterings, dephasing

Coulomb correlations beyond the Bloch equation level

- **Strong Coulomb in ML-TMDC → PL from correlated states**

Auger-Meitner Loss in ML-TMDC

J. Hader and J.V. Moloney, Free Carrier Auger–Meitner Recombination in Monolayer TransitionMetal Dichalcogenides, Nano Letters, Vol. 25, Issue 1, pp. 284-290 (2025)

ML-$MoTe_2$ in air, 300K

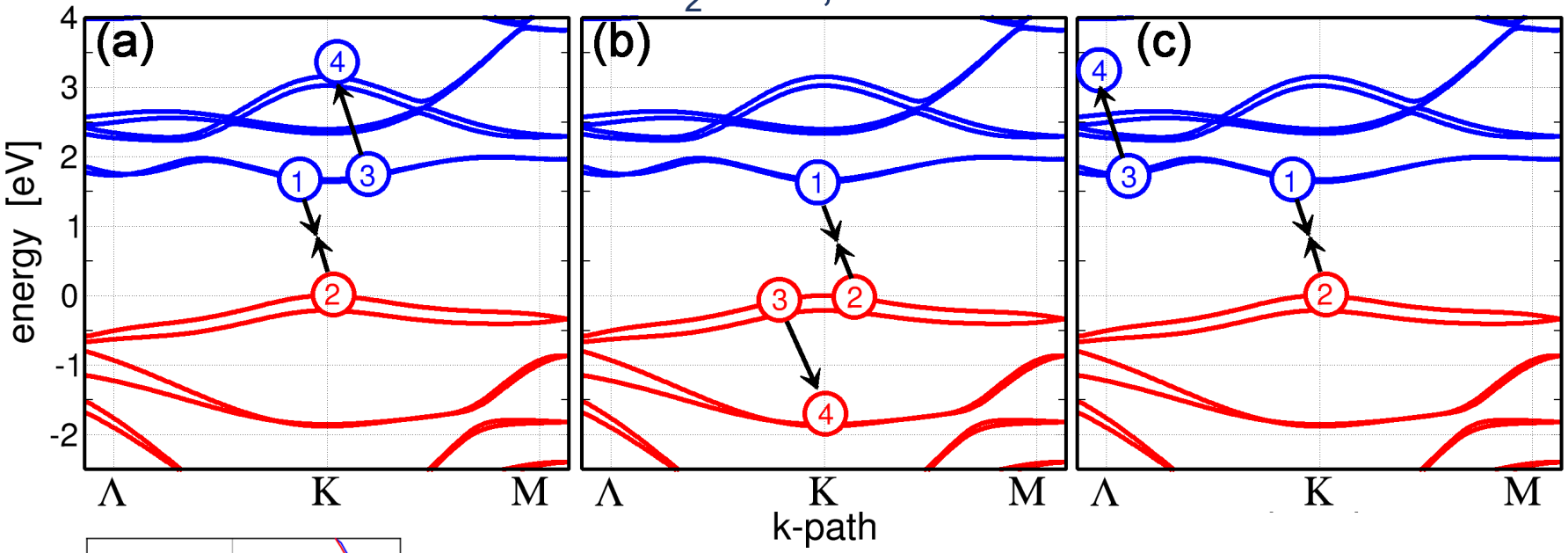

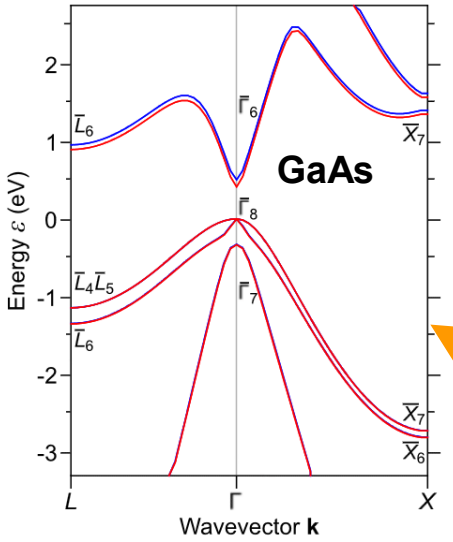

- much stronger Coulomb interaction
- Auger excited carriers can reach higher/lower bands
- strong bandgap renormalizations can bring remote bands into resonance with bandgap

III-V: -- no higher/lower bands can be reached
-- intraband transitions require large momentum transfer
→ weak Coulomb transfer

Auger-Meitner Loss in ML-TMDC

Density- and environment-dependence

ML-MoS_2, 300K
J. Hader, et al.,
Nano Lett. **25**, 284 (2025)

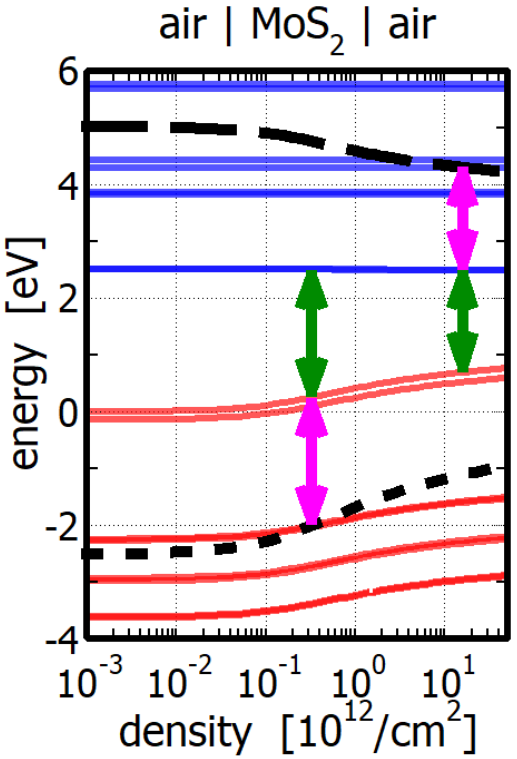

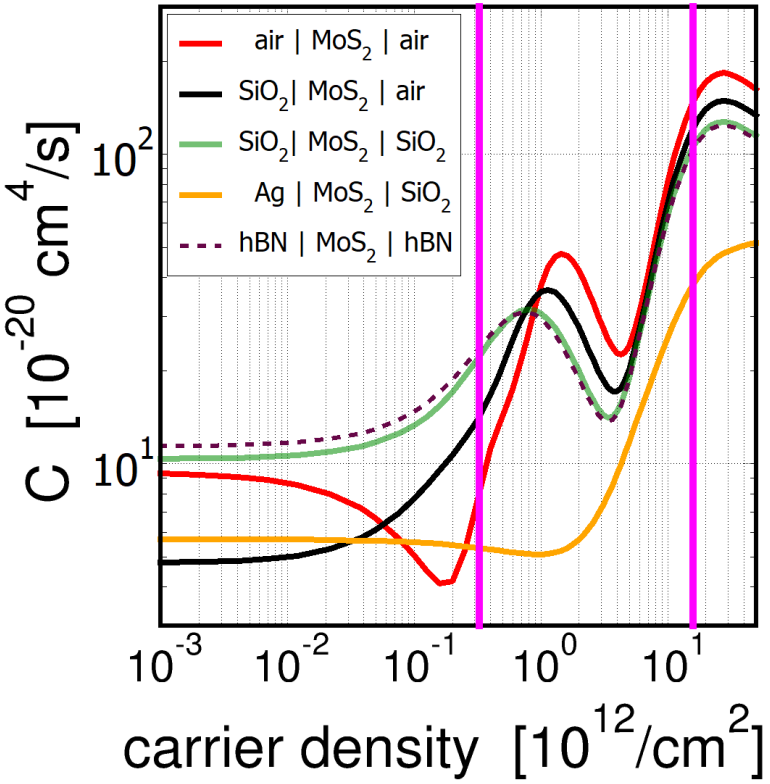

- Loss increases when bands become resonant with gap
- Loss decreases with increased required momentum transfer
- Strong dependence on density and dielectric environment since both influence the bandgap

HHG in ML TMDC, λ = 8 μm; E_0 = 10.24 MV/cm

Coherent carrier motion driven by THz-field:

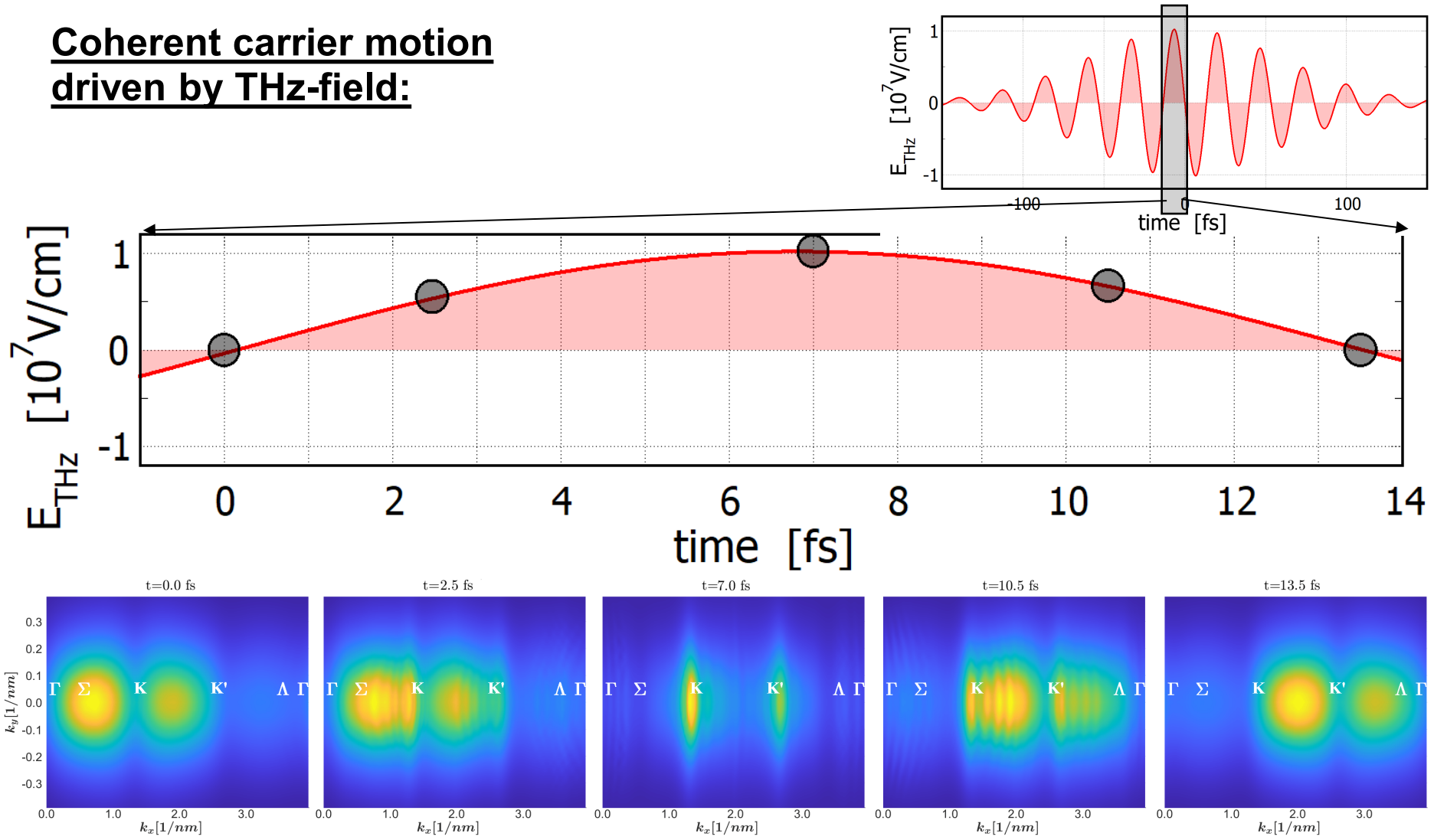

- **carrier distributions vary with optical field on single fs scale**

HHG in ML TMDC, λ = 8 μm; E_0 = 10.24 MV/cm

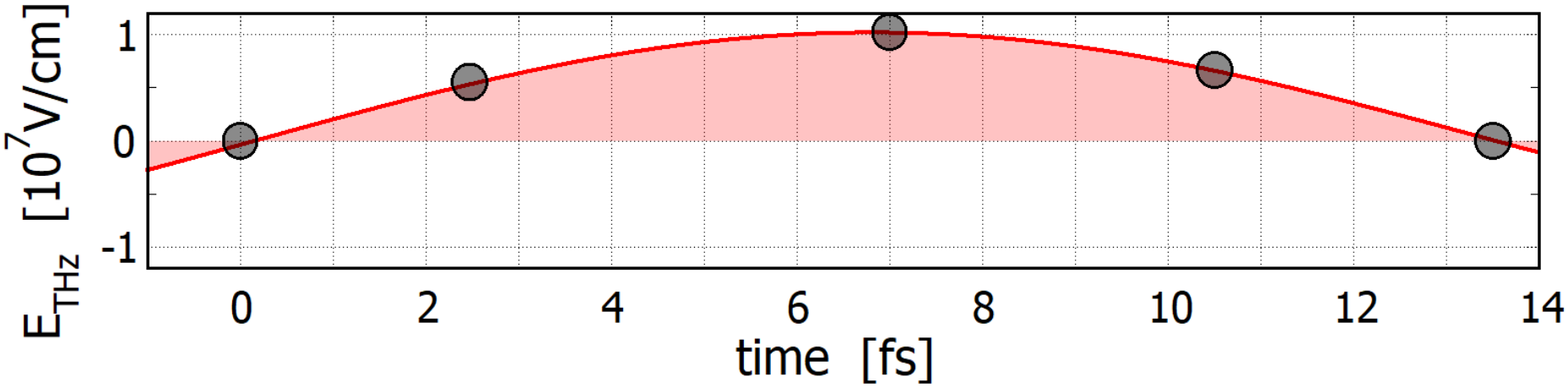

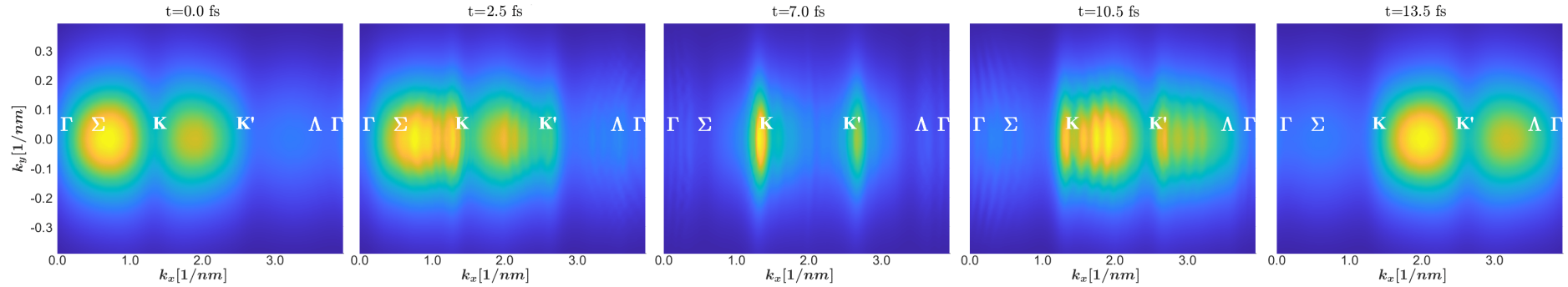

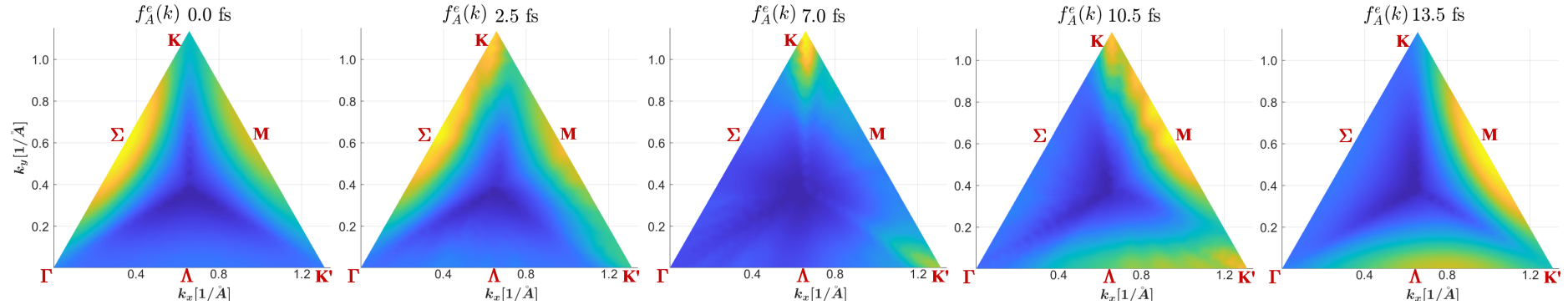

THE UNIVERSITY OF ARIZONA
Wyant College of Optical Sciences

Polarization Dephasing Due to Scatterings

Diagonal scattering contributions corresponding to T_2-time:

$$\frac{\hbar}{\pi}\frac{d}{dt}p_{\mathbf{k}}^{\lambda\mu}\Big|_{corr.} = p_{\mathbf{k}}^{\lambda\mu}\boxed{\frac{1}{T_2(\mathbf{k})}}$$

$$\begin{aligned}
\frac{\hbar}{\pi}\frac{d}{dt}p_{\mathbf{k}}^{\lambda\mu}\Big|_{corr.} = p_{\mathbf{k}}^{\lambda\mu} & \sum_{\substack{i_1\\ \mathbf{q},\mathbf{k}'}} V_{\mathbf{q}}^{i_1\mu\mu i_1} W_{\mathbf{q}}^{i_1\mu\mu i_1} \mathcal{D}\left(\varepsilon_{\mathbf{k}}^{\mu} - \varepsilon_{\mathbf{k}+\mathbf{q}}^{\mu} + \varepsilon_{\mathbf{k}'+\mathbf{q}}^{i_1} - \varepsilon_{\mathbf{k}'}^{i_1}\right)\left[f_{\mathbf{k}'+\mathbf{q}}^{i_1}\left(1 - f_{\mathbf{k}+\mathbf{q}}^{\mu} - f_{\mathbf{k}'}^{i_1}\right) + f_{\mathbf{k}'}^{i_1} f_{\mathbf{k}+\mathbf{q}}^{\mu}\right] - \\
& p_{\mathbf{k}}^{\lambda\mu} \sum_{\substack{i_1\\ \mathbf{q},\mathbf{k}'}} V_{\mathbf{q}}^{i_1\lambda\lambda i_1} W_{\mathbf{q}}^{i_1\lambda\lambda i_1} \mathcal{D}\left(\varepsilon_{\mathbf{k}}^{\lambda} - \varepsilon_{\mathbf{k}+\mathbf{q}}^{\lambda} + \varepsilon_{\mathbf{k}'+\mathbf{q}}^{i_1} - \varepsilon_{\mathbf{k}'}^{i_1}\right)\left[f_{\mathbf{k}'+\mathbf{q}}^{i_1}\left(1 - f_{\mathbf{k}+\mathbf{q}}^{\lambda} - f_{\mathbf{k}'}^{i_1}\right) + f_{\mathbf{k}'}^{i_1} f_{\mathbf{k}+\mathbf{q}}^{\lambda}\right] + \\
& \sum_{\substack{i_1\\ \mathbf{q},\mathbf{k}'}} V_{\mathbf{q}}^{i_1\mu\mu i_1} W_{\mathbf{q}}^{i_1\lambda\lambda i_1} \mathcal{D}\left(\varepsilon_{\mathbf{k}+\mathbf{q}}^{\lambda} - \varepsilon_{\mathbf{k}}^{\lambda} + \varepsilon_{\mathbf{k}'+\mathbf{q}}^{i_1} - \varepsilon_{\mathbf{k}'}^{i_1}\right) p_{\mathbf{k}+\mathbf{q}}^{\lambda\mu}\left[f_{\mathbf{k}'+\mathbf{q}}^{i_1}\left(1 - f_{\mathbf{k}}^{\lambda} - f_{\mathbf{k}'}^{i_1}\right) + f_{\mathbf{k}'}^{i_1} f_{\mathbf{k}}^{\lambda}\right] - \\
& \sum_{\substack{i_1\\ \mathbf{q},\mathbf{k}'}} V_{\mathbf{q}}^{i_1\lambda\lambda i_1} W_{\mathbf{q}}^{i_1\mu\mu i_1} \mathcal{D}\left(\varepsilon_{\mathbf{k}+\mathbf{q}}^{\mu} - \varepsilon_{\mathbf{k}}^{\mu} + \varepsilon_{\mathbf{k}'+\mathbf{q}}^{i_1} - \varepsilon_{\mathbf{k}'}^{i_1}\right) p_{\mathbf{k}+\mathbf{q}}^{\lambda\mu}\left[f_{\mathbf{k}'+\mathbf{q}}^{i_1}\left(1 - f_{\mathbf{k}}^{\mu} - f_{\mathbf{k}'}^{i_1}\right) + f_{\mathbf{k}'}^{i_1} f_{\mathbf{k}}^{\mu}\right] + \\
& p_{\mathbf{k}}^{\lambda\mu} \sum_{\substack{i_1,j_1\\ \mathbf{q},\mathbf{k}'}} V_{\mathbf{q}}^{\mu i_1 i_1\mu} W_{\mathbf{q}}^{\mu j_1 j_1\mu} \mathcal{D}\left(\varepsilon_{\mathbf{k}}^{\mu} - \varepsilon_{\mathbf{k}+\mathbf{q}}^{\mu} + \varepsilon_{\mathbf{k}'}^{j_1} - \varepsilon_{\mathbf{k}'+\mathbf{q}}^{j_1}\right) p_{\mathbf{k}'}^{j_1 i_1} p_{\mathbf{k}'+\mathbf{q}}^{j_1 i_1} - \\
& p_{\mathbf{k}}^{\lambda\mu} \sum_{\substack{i_1,j_1\\ \mathbf{q},\mathbf{k}'}} V_{\mathbf{q}}^{\mu j_1 j_1\mu} W_{\mathbf{q}}^{\mu i_1 i_1\mu} \mathcal{D}\left(\varepsilon_{\mathbf{k}}^{\mu} - \varepsilon_{\mathbf{k}+\mathbf{q}}^{\mu} + \varepsilon_{\mathbf{k}'}^{i_1} - \varepsilon_{\mathbf{k}'+\mathbf{q}}^{i_1}\right) p_{\mathbf{k}'}^{j_1 i_1} p_{\mathbf{k}'+\mathbf{q}}^{j_1 i_1} + \\
& \sum_{\substack{i_1,j_1\\ \mathbf{q},\mathbf{k}'}} V_{\mathbf{q}}^{\mu i_1 i_1\mu} W_{\mathbf{q}}^{j_1\lambda\lambda j_1} \mathcal{D}\left(\varepsilon_{\mathbf{k}+\mathbf{q}}^{\lambda} - \varepsilon_{\mathbf{k}}^{\lambda} + \varepsilon_{\mathbf{k}'}^{j_1} - \varepsilon_{\mathbf{k}'+\mathbf{q}}^{j_1}\right) p_{\mathbf{k}+\mathbf{q}}^{\lambda\mu} p_{\mathbf{k}'}^{j_1 i_1} p_{\mathbf{k}'+\mathbf{q}}^{j_1 i_1} - \\
& \sum_{\substack{i_1,j_1\\ \mathbf{q},\mathbf{k}'}} V_{\mathbf{q}}^{\mu j_1 j_1\mu} W_{\mathbf{q}}^{i_1\lambda\lambda i_1} \mathcal{D}\left(\varepsilon_{\mathbf{k}+\mathbf{q}}^{\mu} - \varepsilon_{\mathbf{k}}^{\mu} + \varepsilon_{\mathbf{k}'}^{j_1} - \varepsilon_{\mathbf{k}'+\mathbf{q}}^{j_1}\right) p_{\mathbf{k}+\mathbf{q}}^{\lambda\mu} p_{\mathbf{k}'}^{j_1 i_1} p_{\mathbf{k}'+\mathbf{q}}^{j_1 i_1} + \\
& \mu \leftrightarrow \lambda, \quad i \leftrightarrow i
\end{aligned}$$

HHG in ML TMDC, λ = 8 μm; E_0 = 10.24 MV/cm

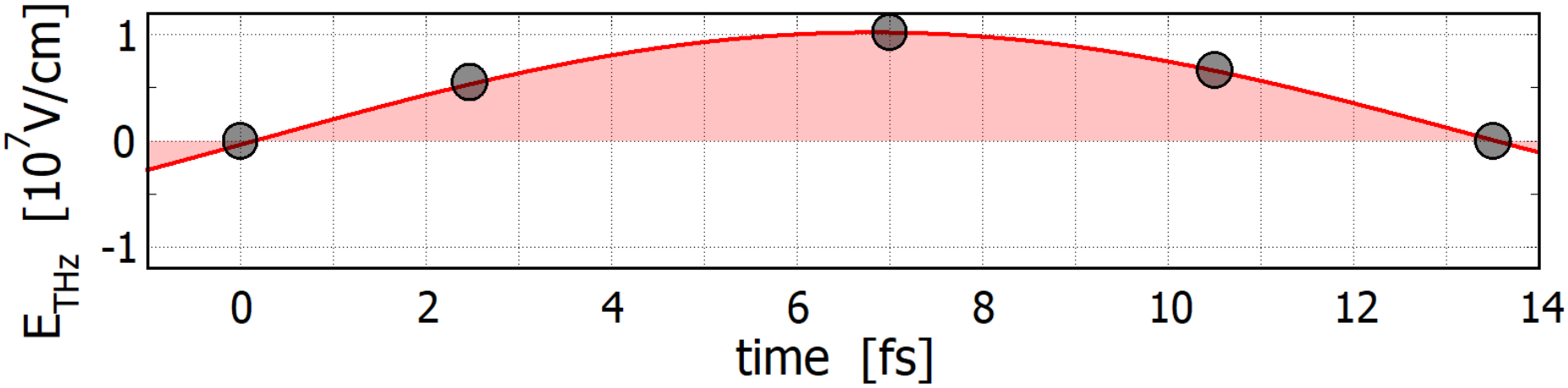

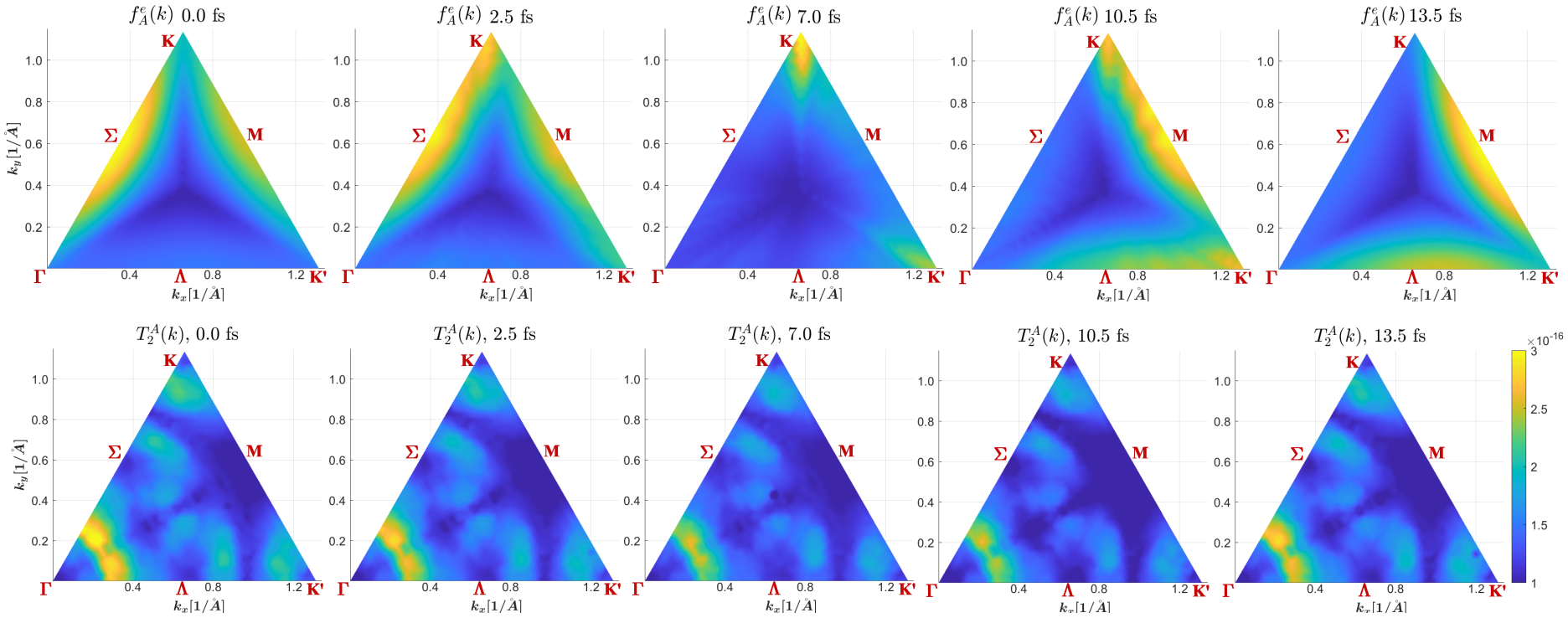

Stratified Structure Propagation Equation (SSPE)

VOLUME 89, NUMBER 28 PHYSICAL REVIEW LETTERS 31 DECEMBER 2002

Unidirectional Optical Pulse Propagation Equation

M. Kolesik, J.V. Moloney, and M. Mlejnek*

$$\partial_t \vec{D}_f(\vec{k}) = -i\omega(\vec{k})\vec{D}_f(\vec{k}) + \frac{i}{2}\omega(\vec{k})[\vec{P}_{NL}(\vec{D},\vec{k}) - \frac{1}{k^2}\vec{k}\vec{k}\bullet\vec{P}_{NL}(\vec{D},\vec{k})]$$

- Restricted to unbounded regions – plane wave modes in M* below.
- No explicit boundary conditions

$$\partial_t \vec{D}(t,k_z,k_\perp) = -i\omega(\vec{k})\vec{D} - \frac{i}{2\mu_0\varepsilon\omega(\vec{k})N}\int(\nabla\nabla\bullet\vec{P} - \Delta\vec{P})M^*(\vec{r}\,|\,k_z k_\perp)dV$$

- M* based on slab boundary conditions needs suitably orthonormalized modes mapped to numerical grid

Extreme NLO with complex driving fields

- N-foil driving field: combine LCP and RCP optical fields with different frequencies: ω and $(N-1)\omega$
  - Combined field will have N-fold rotational+reflection symmetry (in long-pulse limit)

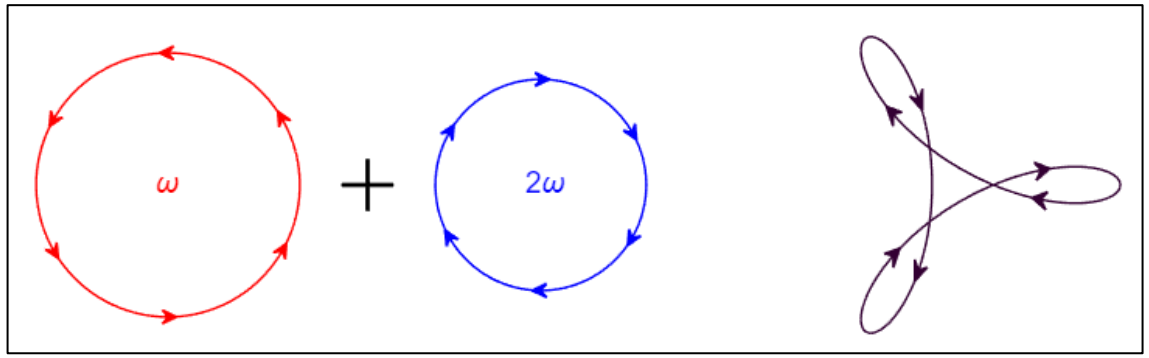

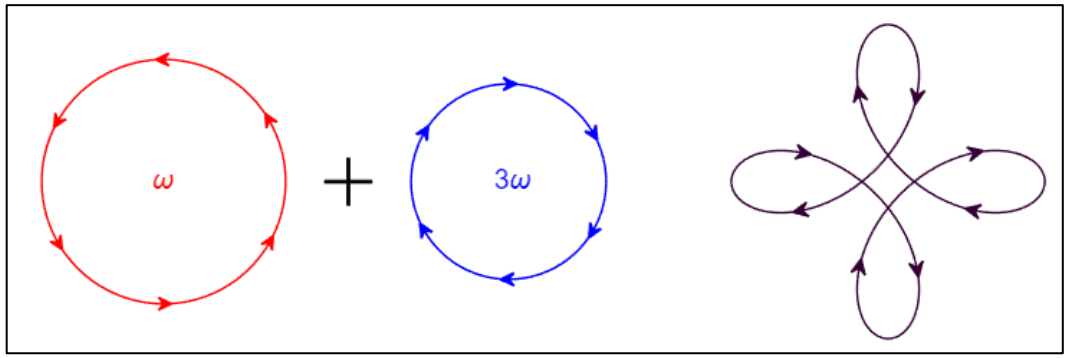

- Polarization vector of pulse has non-trivial time evolution
- Adding higher harmonics can reduce symmetry from D_N to C_N (preserve rotation but remove reflection symmetry)
- How does symmetry of optical field interact with material?
- Our robust SBE solvers can treat complex driving fields in 2D & 3D systems, including materials with non-trivial topology

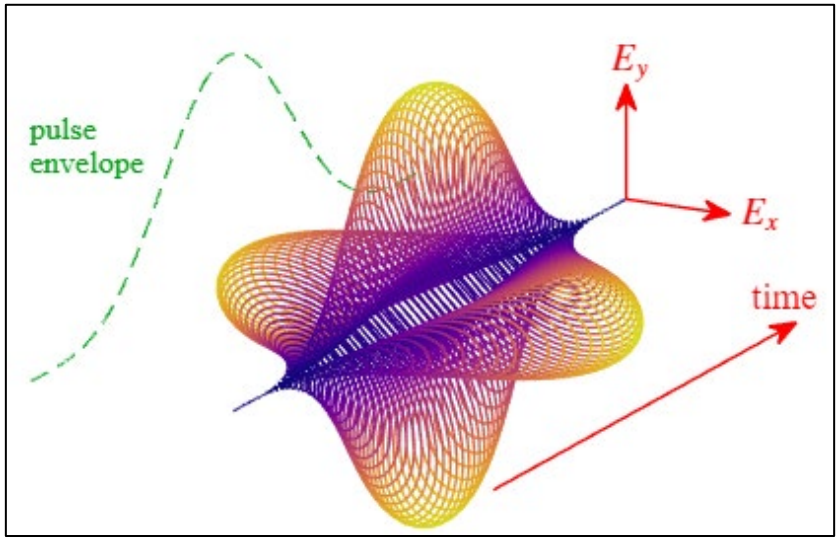

Challenges in Computing Many-Body Correlations

$$\frac{\hbar}{\pi}\frac{\mathrm{d}}{\mathrm{d}t}f_{\mathbf{k}}^{\mathrm{e},i}\bigg|_{\mathrm{corr.}}^{\mathrm{ee}} = \sum_{\substack{i_1,i_2,i_3\\ \mathbf{q},\mathbf{k}'}} V_{\mathbf{q};\mathbf{k}}^{ii_1i_2i_3} W_{\mathbf{q};\mathbf{k}}^{i_3i_2i_1i} \; \mathscr{D}\left(\varepsilon_{\mathbf{k}}^{\mathrm{e},i} + \varepsilon_{\mathbf{k}'-\mathbf{q}}^{\mathrm{e},i_1} - \varepsilon_{\mathbf{k}'}^{\mathrm{e},i_2} - \varepsilon_{\mathbf{k}-\mathbf{q}}^{\mathrm{e},i_3}\right) \left[(1-f_{\mathbf{k}'}^{\mathrm{e},i_2})(1-f_{\mathbf{k}-\mathbf{q}}^{\mathrm{e},i_3})f_{\mathbf{k}}^{\mathrm{e},i}f_{\mathbf{k}'-\mathbf{q}}^{\mathrm{e},i_1} - (1-f_{\mathbf{k}}^{\mathrm{e},i})(1-f_{\mathbf{k}'-\mathbf{q}}^{\mathrm{e},i_1})f_{\mathbf{k}'}^{\mathrm{e},i_2}f_{\mathbf{k}-\mathbf{q}}^{\mathrm{e},i_3}\right]$$

- Energy conserving delta function saves one dimension
- Computational grid points off of uniform grid – linear interpolation of fff, ff and f functions
- 500 speed up with combination of an efficient algorithm and specialized cache friendly hardware

$$\iiint_{\Omega} \kappa(A,C,E)\; f_A f_C f_E \; \mathrm{d}\Omega = [(f_b - f_a)\alpha + f_a]\cdot[(f_d - f_c)\beta + f_c]\cdot[(f_f - f_e)\gamma + f_e]$$

constant

$$= f_a f_c f_e \cdot [-\alpha\beta\gamma - \alpha\beta - \alpha\gamma - \beta\gamma - \alpha - \beta - \gamma - 1] + \bullet\bullet\bullet\bullet\bullet$$

$$= f_a f_c f_e w_{\mathrm{Total}}$$

- Algorithm: Precompute factored, sorted and accumulate weights – factor of 50 speed up

Algorithm and Hardware Acceleration – Many-body Correlations

Weights file is:

- 1D and sequentially ordered
- takes maximum advantage of CPU multi-level caches
- optimally ordered for Advanced Vector Extensions (AVX) in modern CPUs
    - Each AVX-512 Vector register performs 8 double precision floating point operations **per CPU clock cycle**

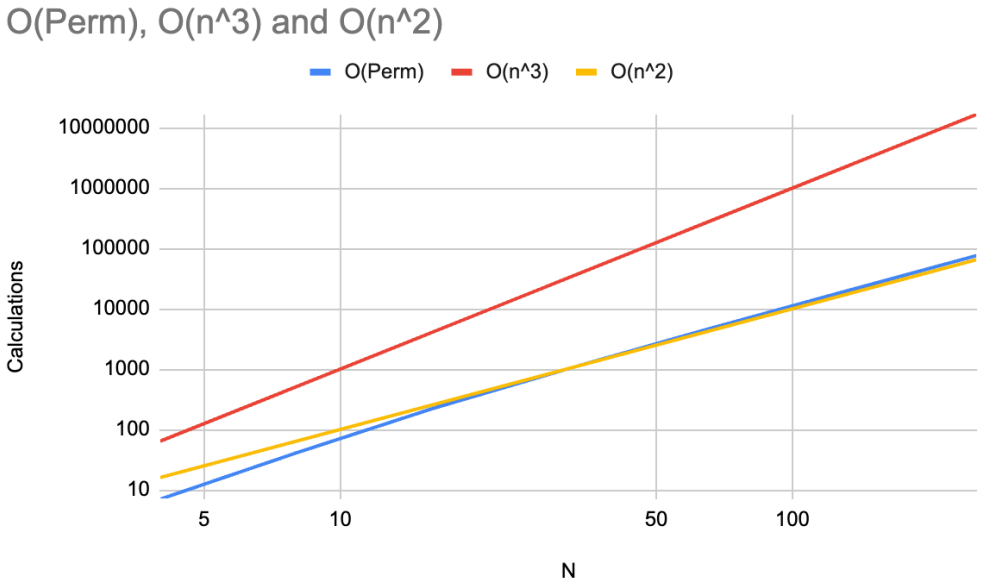

We tested the performance on a number of INTEL and AMD 64Core CPUs and a range of nVidia GPUs

- In initial tests we see a average speed of 50 on CPUs and 500 on GPUs over a naïve hand coded implementation

Summary of Future Challenges

- Build a computational framework that rigorously captures nonlinear, nonequilibrium interactions in finite solids
- Design computationally feasible gauge invariant SBE sources that faithfully capture the symmetry, gauge invariance,…
- Evaluate and incorporate many-body correlations into the simulation framework
- Design algorithms that exploit new hardware accleration

Publications 2024

S. Tsaoussis, S. Addamane, R. J. Jones, and J. V. Moloney, "Dual-wavelength channel GHz repetition rate mode-locked VECSEL cavities sourced from a common gain medium," Optics Letters Vol. 49, Issue 7, pp. 1688-1691, (2024)

A. M. Parks, J. V. Moloney, and T. Brabec, "Bloch gauge symmetry of the semiconductor Bloch equations [Invited]," J. Opt. Soc. Am. B 41, B47-B59 (2024)

J. Hader and J.V. Moloney, "Photo Luminescence and Radiative Carrier Losses in Monolayer Transition Metal Dichalcogenides," Nano Lett. 2024, Vol. 24, Issue 17, pp. 5231-5237 (2024)

M. Hastings, P. Panagiotopoulos, M. Kolesik, and J.V. Moloney, "Multiharmonic Spanning Nonlinear X-wave: An Asymptotic State of Extreme Long Wave Infrared Dispersive Shock Regularization", Phys. Rev. Lett. Vol. 132, Issue 25, 253801 (2024)

J. Hader and J.V. Moloney, "Free Carrier Auger–Meitner Recombination in Monolayer Transition Metal Dichalcogenides," Nano Letters, Vol. 25, pp. 284-290 (2025)

M. Kolesik, “Sample-orientation effects in solid-state high-harmonic generation: computational study of GaAs,” J. Opt. Soc. Am. B 41, B7-B13 (2024)

S. Ya. Tochitsky et al. "Self-channeling of a multi-Joule 10 μm picosecond pulse train through long distances in air," Optics Express, Vol. 32, Issue 2, pp. 2067-2080, (2024)

A. M. Parks, J. V. Moloney, and T. Brabec, "Bloch gauge symmetry of the semiconductor Bloch equations [Invited]," J. Opt. Soc. Am. B 41, B47-B59 (2024)

Semiconductor Luminescence Equations

Equation of motion for excitonic correlations:

$$
\begin{aligned}
i\hbar\frac{\partial}{\partial t}C^{i'jij'}_{\mathbf{k},\mathbf{k}'} = & \sum_{i'',i''',j'',j'''}\left[\left(\mathcal{E}^{ii''}_{\mathbf{k}}\delta_{i'i'''}-\mathcal{E}^{i'i'''}_{\mathbf{k}'}\delta_{ii''}\right)\delta_{jj''}\delta_{j'j'''}+\left(\mathcal{E}^{jj''}_{\mathbf{k}}\delta_{j'j'''}-\mathcal{E}^{j'j'''}_{\mathbf{k}'}\delta_{jj''}\right)\delta_{i'i'''}\delta_{ii''}\right]C^{i'''j''i''j'''}_{\mathbf{k},\mathbf{k}'} \\
& +V^{ij'ji'}_{\mathbf{k}'-\mathbf{k}}\left[f^{j}_{\mathbf{k}}f^{i}_{\mathbf{k}}\left(1-f^{j'}_{\mathbf{k}'}\right)\left(1-f^{i'}_{\mathbf{k}'}\right)-f^{j'}_{\mathbf{k}'}f^{i'}_{\mathbf{k}'}\left(1-f^{j}_{\mathbf{k}}\right)\left(1-f^{i}_{\mathbf{k}}\right)\right] \\
& +\left(1-f^{i'}_{\mathbf{k}'}-f^{j'}_{\mathbf{k}'}\right)\sum_{i'',j'',\mathbf{k}''}V^{j'i''i'j''}_{\mathbf{k}'-\mathbf{k}''}C^{i''jij''}_{\mathbf{k},\mathbf{k}''}-\left(1-f^{i}_{\mathbf{k}}-f^{j}_{\mathbf{k}}\right)\sum_{i'',j'',\mathbf{k}''}V^{ij''ji''}_{\mathbf{k}-\mathbf{k}''}C^{i'j''i''j'}_{\mathbf{k}'',\mathbf{k}} \\
& -2\sum_{k''}\left\{\left[\tilde{\Gamma}^{j'\star}_{\mathbf{k}',\mathbf{k}''}+\tilde{\Gamma}^{i'\star}_{\mathbf{k}',\mathbf{k}''}\right]C^{i'jij'}_{\mathbf{k},\mathbf{k}''}+\left[\tilde{\Gamma}^{j}_{\mathbf{k},\mathbf{k}''}+\tilde{\Gamma}^{i}_{\mathbf{k},\mathbf{k}''}\right]C^{i'jij'}_{\mathbf{k}'',\mathbf{k}'}\right\}.
\end{aligned}
$$

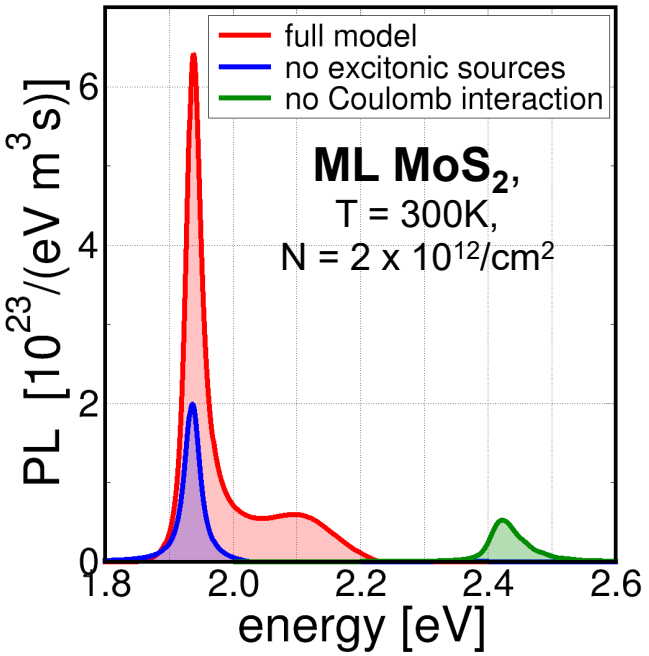

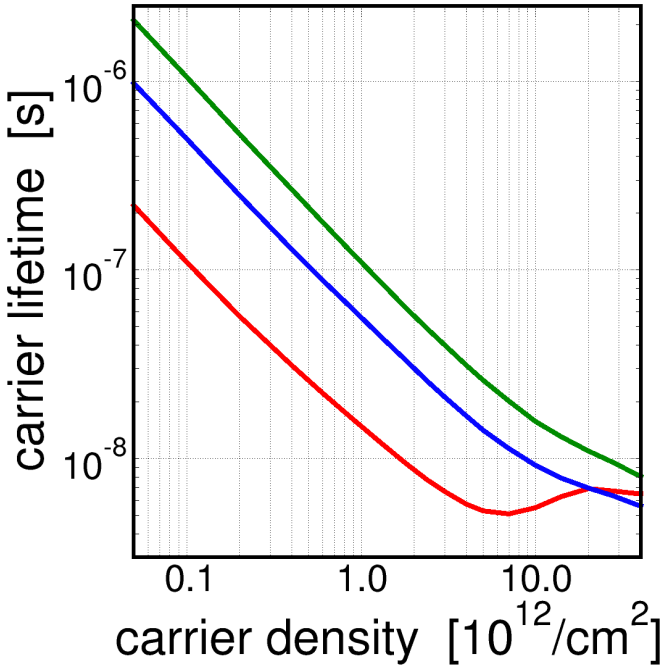

- **Coulomb correlations beyond Hartree-Fock dominate PL and radiative carrier lifetimes**

Shortcomings of T_2-Approximation

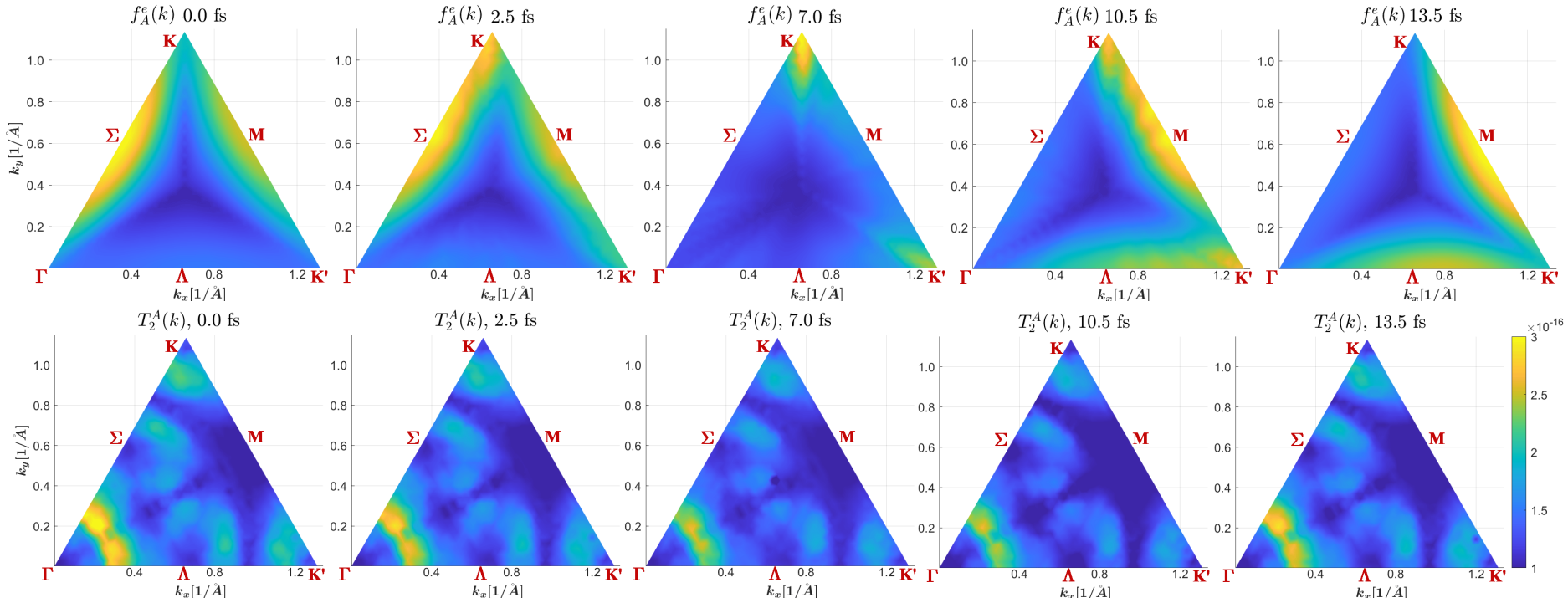

- **Unrealistically short dephasing times of tenths of fs due to neglect of compensation between diagonal and off-diagonal terms**
- **Missing dephasing due to polarization interferences**
- **Use of static screening can create unphysical singularities in case of non-equilibrium distributions:**

$$W_q = \frac{1}{\epsilon(q,\omega)} V_q, \quad \epsilon_q = 1 - V_q \sum_k \frac{f_{k-q} - f_k}{\varepsilon_{k-q} - \varepsilon_k}$$

can be positive or negative in non-equilibrium

Transverse Spatial Gratings

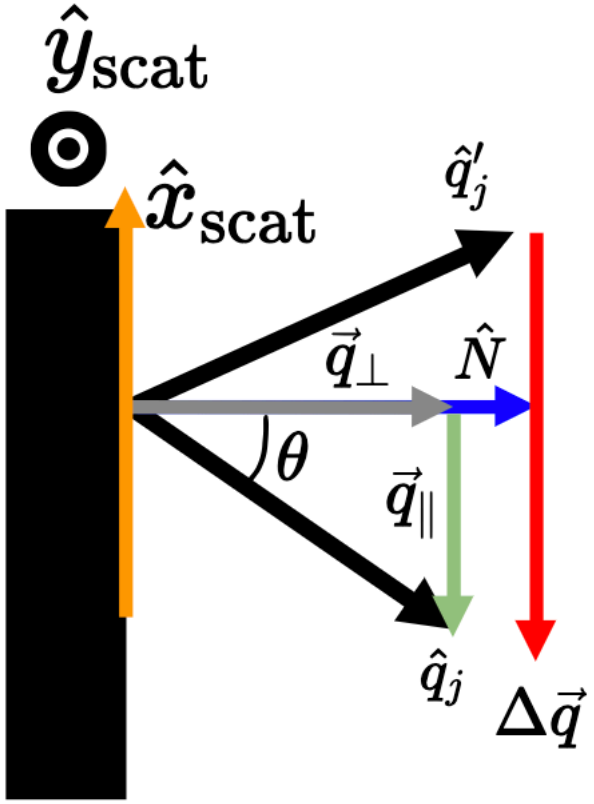

Defining the Grating Directions:

$$\hat{g}_q = \frac{\vec{\nabla}g \times \hat{N}}{|\vec{\nabla}g \times \hat{N}|}$$

$$\hat{g}_p = \frac{\vec{\nabla}g \times \hat{N} \times \hat{N}}{|\vec{\nabla}g \times \hat{N}|}$$

Grating Period: $\Lambda = \frac{\lambda}{2|\vec{q}_{||}|}$

Grating Direction: $\hat{g}_p = \frac{\vec{q}_{||}}{|\vec{q}_{||}|}$

Period Vector: $\vec{\nabla}g = \hat{g}_p\Lambda = \Lambda\frac{\vec{q}_{||}}{|\vec{q}_{||}|}$

$$s_p = \hat{g}_p \cdot \hat{q}_j + \frac{m\lambda}{\left|\vec{\nabla}g \times \hat{N}\right|} \qquad s_q = \hat{g}_q \cdot \hat{q}_j$$

Generalized : $\hat{q}'_m = s_p\hat{g}_p + s_q\hat{g}_q + \sqrt{1 - s_p^2 - s_q^2}\,\hat{N}$

Single plane: $\hat{q}'_m = (1+2m)\vec{q}_{||} + \sqrt{1 - \left|\vec{q}_{||}\right|^2 (1+2m)^{\,2}}\hat{N}$

Auger-Meitner Loss in ML-TMDC

Density- and bandgap-dependence

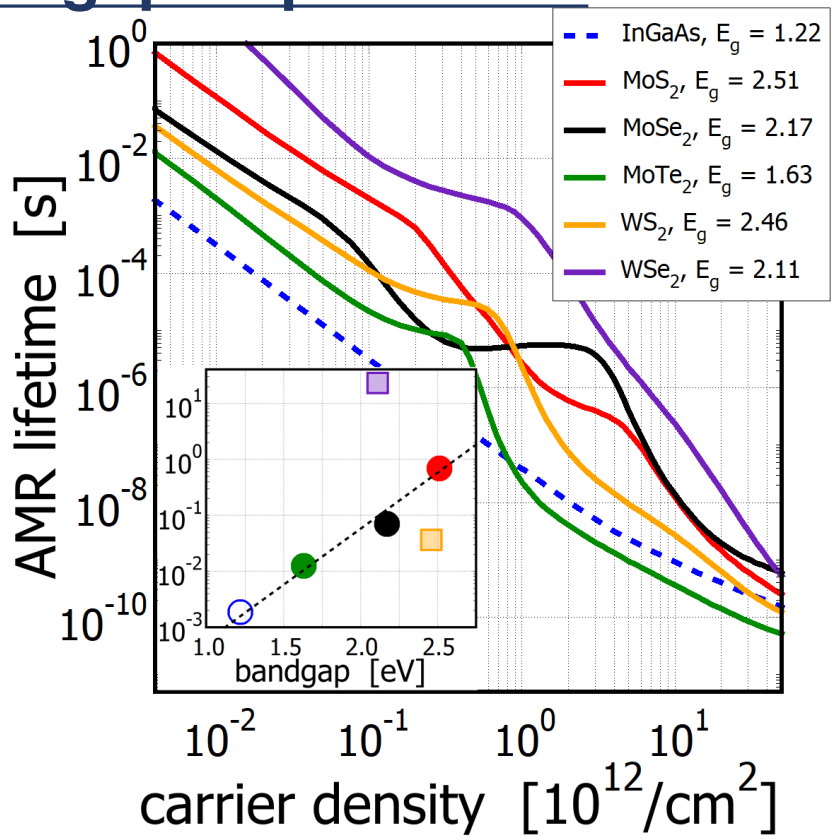

TMDC in air, 300K

J. Hader, et al., Nano Lett. **25**, 284 (2025)

- Auger losses show similar dependence on bandgap as III-V materials
- Auger loss magnitude similar to conventional III-V materials for similar wavelengths despite much stronger Coulomb interaction.
- Density dependence more complicated due to resonant higher bands